

A Foundational Potential Energy Surface Dataset for Materials

Aaron D. Kaplan,^{†,⊥} Runze Liu,^{‡,⊥} Ji Qi,^{‡,⊥} Tsz Wai Ko,[‡] Bowen Deng,^{¶,†}
Janosh Riebesell,^{†,§} Gerbrand Ceder,[†] Kristin A. Persson,^{||,†} and Shyue Ping
Ong^{*,‡}

[†]*Materials Sciences Division, Lawrence Berkeley National Laboratory, Berkeley, California
94720, United States*

[‡]*Aiiso Yufeng Li Family Department of Chemical and Nano Engineering, University of
California San Diego, 9500 Gilman Dr, Mail Code 0448, La Jolla, CA 92093-0448, United
States*

[¶]*Department of Materials Science and Engineering, University of California, Berkeley,
California 94720, United States*

[§]*Cavendish Laboratory, University of Cambridge, J. J. Thomson Ave, Cambridge, UK*

^{||}*Department of Materials Science and Engineering, University of California, Berkeley, CA
94720, USA*

[⊥]*These authors contributed equally to this work.*

E-mail: ongps@ucsd.edu

Abstract

Accurate potential energy surface (PES) descriptions are essential for atomistic simulations of materials. Universal machine learning interatomic potentials (UMLIPs)¹⁻³ offer a computationally efficient alternative to density functional theory (DFT)⁴ for

PES modeling across the periodic table. However, their accuracy today is fundamentally constrained due to a reliance on DFT relaxation data.^{5,6} Here, we introduce MatPES, a foundational PES dataset comprising $\sim 400,000$ structures carefully sampled from 281 million molecular dynamics snapshots that span 16 billion atomic environments. We demonstrate that UMLIPs trained on the modestly sized MatPES dataset can rival, or even outperform, prior models trained on much larger datasets across a broad range of equilibrium, near-equilibrium, and molecular dynamics property benchmarks. We also introduce the first high-fidelity PES dataset based on the revised regularized strongly constrained and appropriately normed (r^2 SCAN) functional⁷ with greatly improved descriptions of interatomic bonding. The open source MatPES initiative emphasizes the importance of data quality over quantity in materials science and enables broad community-driven advancements toward more reliable, generalizable, and efficient UMLIPs for large-scale materials discovery and design.

Electronic structure methods, such as those based on Kohn-Sham DFT,⁴ provide the most accurate descriptions of the PES. However, DFT typically scales with the number of electrons cubed, making it prohibitively expensive for simulating complex materials requiring models with large numbers of atoms (e.g., low-symmetry interfaces, amorphous materials, etc.) or properties requiring long time-scale statistics (e.g. diffusivity). To overcome this limitation, an interatomic potential (IP), also known as a force field, is often used to approximate the PES with linear scaling with respect to the number of atoms. Classical IPs, where a functional form is prescribed,^{8,9} sacrifice substantial accuracy and are limited to a particular chemical identity and bond regime.¹⁰

Machine learning IPs (MLIPs) have emerged as a computationally efficient way to bridge the gap between DFT and classical IPs by using an ML model to learn the DFT PES for different configurations of atoms.^{11,12} By explicit construction, message passing, or both, MLIPs can capture multi-body interactions to simulate diverse bonding. Among MLIP architectures, graph-based architectures^{1,2,13,14} have a distinct advantage in handling systems of high compositional complexity by using a unique learned embedding vector¹ to repre-

sent each unique element. State-of-the-art architectures typically combine message-passing graphs with many-body interactions^{1,2,15} to achieve an optimal balance between flexibility and efficiency.

In the past two years, a special class of *universal* MLIPs (UMLIPs)¹⁻³ have emerged with nearly complete coverage of the periodic table. UMLIPs can potentially serve as a drop-in replacement for expensive DFT calculations in a wide range of applications, such as structural relaxations, molecular dynamics (MD) simulations, prediction of PES-derived properties such as phonon dispersions, elastic constants, etc.

However, present UMLIPs are still limited in their accuracy, especially compared to custom-fitted MLIPs. This can be attributed to three major limitations in often employed data sets. For example, the Materials Project⁵ structural relaxation dataset (MPF¹ or MPtrj,² here referred to collectively as “MPRelax”) is the most commonly used dataset to train UMLIPs,¹⁶ but the rationale for the dataset’s creation over the past decade did not prioritize PES accuracy. First, the MPRelax dataset comprises mostly near-equilibrium structures and therefore can only inform the shape of the PES directly adjacent to a minimum. Second, the MPRelax dataset mixes calculations using the Perdew-Burke-Ernzerhof (PBE)¹⁷ generalized gradient approximation (GGA) exchange-correlation functional without and with a Hubbard U (PBE+ U) parameter, which are then empirically adjusted to reproduce experimental formation energies.¹⁸ The forces and stresses computed using PBE and PBE+ U also differ,¹⁹ but remain unadjusted, resulting in a mismatch between the treatment of PES quantities. This opens the possibility for non-smooth features in the PES when moving between distinct chemical spaces trained on PBE and PBE+ U data. Finally, the computational settings used in MPRelax and other datasets⁶ were chosen to balance computational cost and accuracy in high-throughput structural relaxation workflows, with changes reflecting improvements in DFT methodology made over the course of more than a decade.

The end result is that the MPRelax data contains significant systematic and unsystematic noise in its description of PESs. Qi et al.²⁰ demonstrated that the substitution of noisy

PES data with accurate single-point DFT calculations can improve the accuracy of UMLIPs, as well as their reliability in molecular dynamics (MD) simulations. Deng et al.²¹ have also found that current UMLIPs tend to underpredict larger-magnitude interatomic forces and over-soften phonons, which is likely due to under-sampling of off-equilibrium local environments (i.e., those farther from the PES minimum).

There have been efforts to go beyond the limitations of the MPRelax dataset through brute-force data generation, most notably by industry research groups.²²⁻²⁴ For instance, Meta recently released the Open Materials 2024 (OMat24) dataset,²⁴ which comprises around 100 million structures. However, with the notable exception of OMat24, industry datasets are usually closed source^{22,23} and inaccessible to the wider research community. Training with such immense datasets also requires resources beyond those readily available at public computing centers.

Here, we report the launch of MatPES, an open science initiative to develop a foundational PES dataset for materials. In addition to remedying the historical dependencies of the MPRelax set, we also improve upon the underlying DFT description of the PES. The PBE functional, predominantly used by UMLIP efforts, tends to underestimate the strength of weaker ionic and van der Waals bonds;²⁵ more accurate meta-GGAs, such as the revised regularized strongly constrained and appropriately normed (r²SCAN) functional,⁷ have been developed that are better able to capture differences in local electronic bonding²⁶ and describe intermediate van der Waals bonding without an explicit dispersion correction.²⁷ The initial MatPES dataset (version 2025.1) comprises accurate energies, forces, and stresses from well-converged single-point PBE and r²SCAN calculations of 504,811 equilibrium and non-equilibrium structures, generated using the workflow depicted in Fig. 1. We demonstrate that MatPES-trained UMLIPs significantly outperform MPRelax- and OMat24-trained UMLIPs on a broad range of equilibrium, near-equilibrium and dynamic properties. This dataset is publicly available on a dedicated web site (<http://matpes.ai>), as well as through the Materials Project MPContribs platform,²⁸ and the pre-trained UMLIPs are released in the

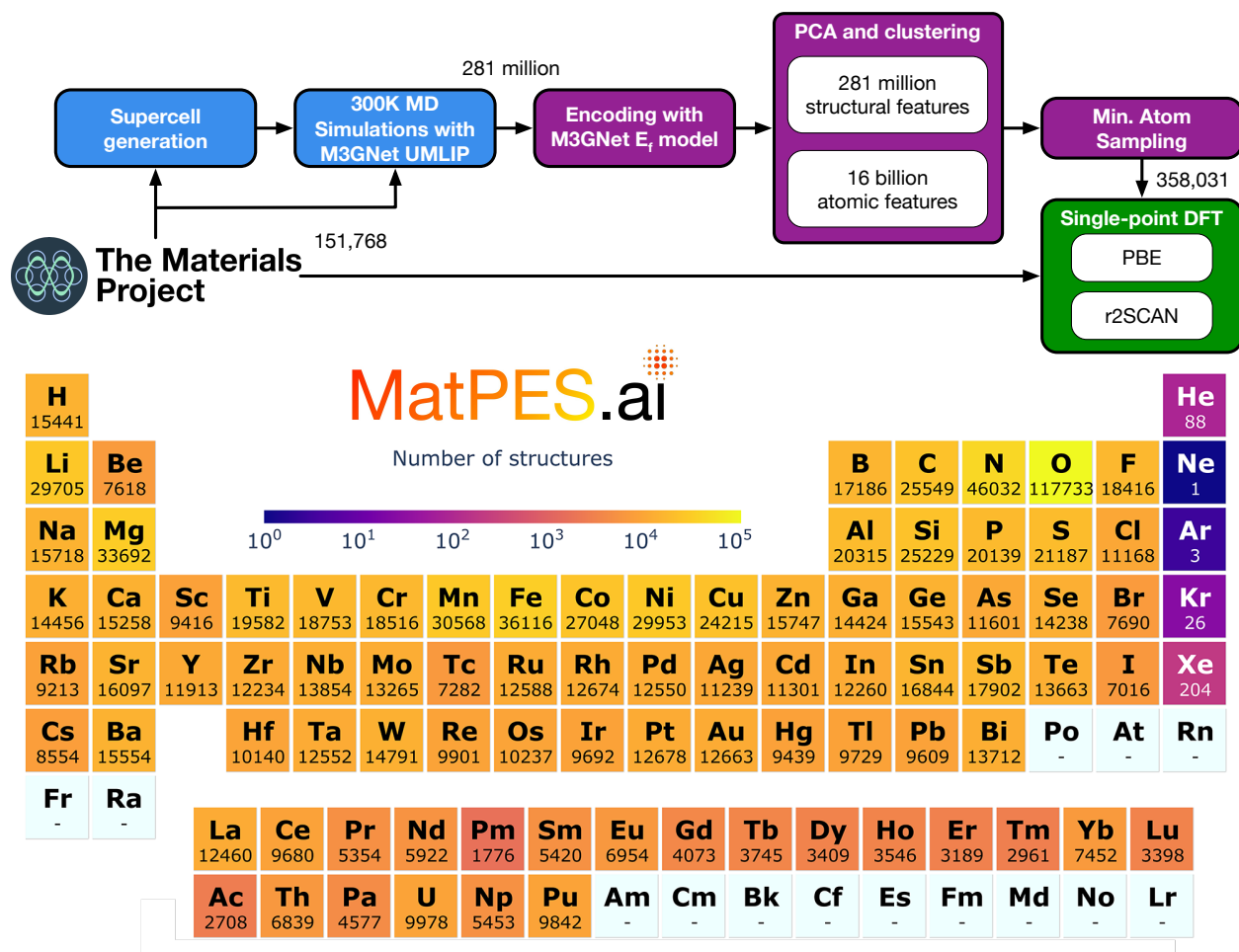


Fig. 1: MatPES dataset development workflow. The number of structures at each stage in the workflow is indicated. A comprehensive configuration space was generated by performing NpT MD simulations at 300K and 1 atm on 281,572 ground-state structures and supercells obtained from the Materials Project (v2022.10.28)⁵ using a pre-trained M3GNet UMLIP (version MP-2021.2.8-DIRECT). A 2-stage Dimensionality-Reduced Encoded Clusters with sTratified (2DIRECT) sampling²⁰ was then used to extract representative structures from a configuration space of ~ 281 million structures with ~ 16 billion atomic environments. In each cluster, the structure with the smallest number of atoms was selected to minimize the computational burden. The MD dataset was then augmented with ground-state structures with < 100 atoms per cell from the Materials Project to ensure coverage of equilibrium local environments. Single-point DFT calculations with stringent energy and force convergence parameters were then performed on all 504,811 structures. The periodic table heatmap indicates the number of structures containing each element and is colored on a logarithmic scale. The MatPES r²SCAN dataset has similar elemental distribution (Fig. S6).

Results

Dataset composition

The MatPES v2025.1 dataset comprises a total of 434,712 PBE and 387,897 r²SCAN calculations, with a comprehensive and relatively well-balanced coverage of all elements of the periodic table (Fig. 1 and Fig. S6a). With the exception of inert noble gases, unstable radioactive elements, and the rare earths, each element has at least 7,000 structures. The extremely large number of structures with oxygen reflects the myriad technologically relevant oxides in the Materials Project database. There are two crucial differentiators in how the MatPES dataset was constructed that yield significant advances over previously reported datasets.

First, the structures in the MatPES dataset were sampled from an extremely large configuration space of 281 million structures and 16 billion atomic environments from 300K MD simulations of unit cells *and* supercells with a pre-trained Materials 3-body Graph Network (M3GNet) UMLIP (see Methods). We found the use of supercells to be of critical importance, as they cover a wider range of atomic environments than unit cells in MD simulations (Fig. S8). Prior datasets are derived almost entirely from small unit cells due to the use of expensive DFT methods in configuration space generation.

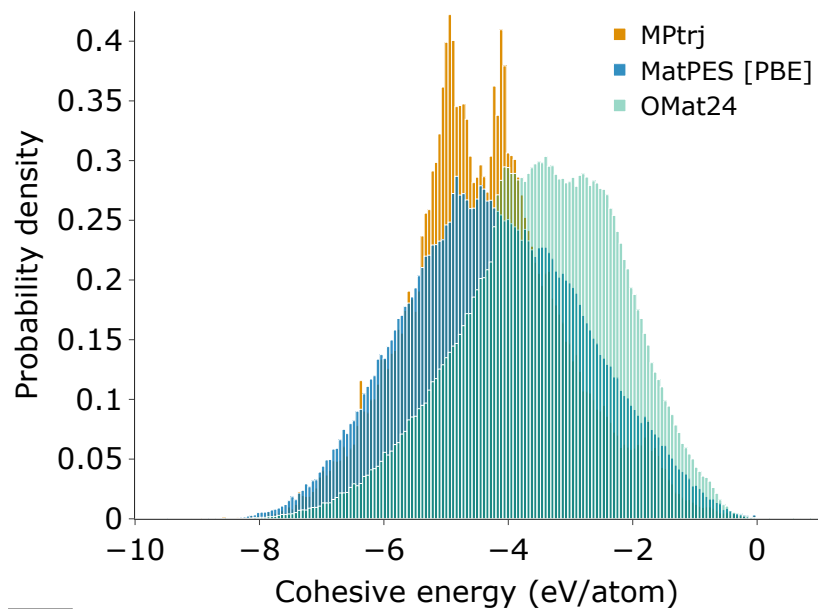
Second, we developed an enhanced 2-stage version of the Dimensionality-Reduced Encoded Clusters with sTratified (2DIRECT) sampling²⁰ approach to ensure data-efficient coverage of this configuration space. Briefly, each structure was encoded using a pre-trained M3GNet formation energy model.¹ The intermediate output of the readout layer and the updated node features after the first graph convolution were then extracted as the structural and atomic/local environment features, respectively. Then a two-step principal component analysis (PCA) and clustering were carried out in the structural feature followed by the

atomic feature space. This 2DIRECT sampling approach ensures that the MatPES dataset covers the entire space of structural and atomic environments in a data-efficient manner. The result is that the MatPES dataset is only a fraction of the size and yet samples a much larger space of structures compared to the MPtrj dataset (Fig. S7).

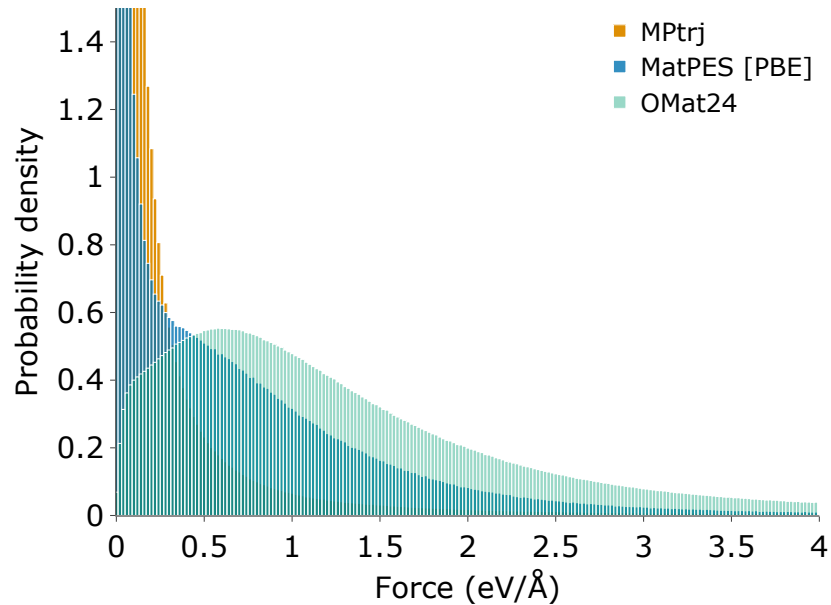
Compared to both MPtrj and OMat24, the MatPES PBE dataset has a more Gaussian-like distribution of cohesive energies per atom E_{coh} (Fig. 2b) and a log-normal-like distribution of interatomic force magnitudes $|\mathbf{F}_i|$ (Fig. 2c). Here, we have chosen E_{coh} (Eq. 1) as a more appropriate measure of the overall quality of the dataset than the formation energy that is often used in the literature. E_{coh} measures the stability of a solid relative to its atomic constituents and should always have a negative value except in cases of poor energy convergence or structures with unphysical bond configurations (e.g., excessively short bond distances). By including structures from 300K MD simulations, the MatPES PBE dataset samples a much wider range of E_{coh} and $|\mathbf{F}_i|$ than the MPtrj dataset. The $|\mathbf{F}_i|$ distribution of the MPtrj dataset is especially narrow, reflecting its lack of coverage of local environments farther away from equilibrium. The OMat24 dataset has a much greater fraction of structures with higher E_{coh} and $|\mathbf{F}_i|$, as it was constructed from hypothetical structures in the Alexandria PBE database.⁶ Furthermore, OMat24 under-samples near-equilibrium local environments by sampling structures only from *ab initio* MD (AIMD). Overall, the MatPES dataset achieves a better balance of on- and off-equilibrium structures and local environments. The MatPES r²SCAN dataset has similar E_{coh} and $|\mathbf{F}_i|$ distributions as the MatPES PBE dataset (Fig. S6).

PES benchmarks

UMLIPs were trained using MatPES PBE and r²SCAN datasets using three graph-based architectures: M3GNet,¹ Crystal Hamiltonian Graph Network (CHGNet),² and TensorNet¹⁴ (see Methods). In addition, we have trained M3GNet and CHGNet UMLIPs using the MPF and MPtrj datasets, respectively, and TensorNet UMLIPs using the MPF and OMat24



(a)



(b)

Fig. 2: Coverage of the MatPES PBE dataset. Distribution of PBE **a**, cohesive energies (E_{coh}) and **b**, interatomic force magnitudes ($|\mathbf{F}_i|$) in the MatPES (blue), MPtrj (orange),² and OMat24 (yellow)²⁴ datasets. The composition of the datasets are as follows: MatPES PBE: 434,712 structures (326,635 MD snapshots, 108,077 MP equilibrium structures); MPtrj: 1,580,361 structures from MP relaxations; OMat24: 1,077,382 structures. The MPtrj and OMat24 datasets contain a mixture of PBE and PBE+ U data, whereas MatPES PBE contains only PBE data.

datasets to ensure a consistent basis for comparison. These architectures were selected to evaluate the performance of MatPES on both symmetry-invariant (M3GNet and CHGNet) and equivariant (TensorNet) models. All three architectures are implemented in the common Materials Graph Library (MatGL)²⁹ to ensure consistency in parameter optimization. Although the authors are aware of other architectures in the literature, a comprehensive evaluation of different architectures is beyond the scope of this work. Furthermore, subsequent results will show that the differences in performance between different architectures are relatively small compared to those between different datasets.

Table 1: Mean absolute errors (MAEs) in PES quantities for trained UMLIPs. The energies, force, stress, and magnetic moment (magmom) MAEs are reported in units of meV atom⁻¹, meV Å⁻¹, GPa, and μ_B , respectively. The magmom is only used in the training of the CHGNet UMLIPs. The numbers are reported in the order of training/validation/test MAEs. The training, validation, and test sets are randomly selected from the complete dataset in proportions of 90%:5%:5%, respectively.

UMLIP	Energy	Force	Stress	Magmom
MatPES PBE				
M3GNet	40/45/45	155/177/181	0.734/0.898/0.888	N/A
CHGNet	27/32/31	81/124/136	0.375/0.617/0.642	0.066/0.067/0.066
TensorNet	33/36/36	121/138/148	0.602/0.695/0.700	N/A
MatPES r²SCAN				
M3GNet	38/45/44	172/208/210	0.774/0.982/0.970	N/A
CHGNet	26/27/30	86/150/156	0.359/0.705/0.735	0.067/0.066/0.072
TensorNet	32/34/34	139/163/163	0.653/0.754/0.754	N/A
MPF				
M3GNet	20/23/334	63/72/297	0.259/0.399/2.026	N/A
TensorNet	29/29/316	78/83/289	0.361/0.471/1.984	N/A
MPtrj				
CHGNet	26/30/698	49/70/265	0.173/0.297/1.872	0.036/0.037/0.038
OMat24				
TensorNet	23/26/202	111/116/186	0.565/0.584/1.151	N/A

The training and validation MAEs in PES quantities (energies, forces, stresses) of the MatPES UMLIPs are slightly larger than those of the MPRelax or OMat24 UMLIPs of the same architecture (Table 1). This can be attributed to the greater proportion of structures with larger forces and stresses in the MatPES dataset (Fig. 2). However, the MatPES PBE

UMLIPs significantly outperform the MPRelax and OMat24 trained UMLIPs in terms of the MAEs on the test set, which comprises 21,737 structures (5%) randomly sampled from the entire MatPES dataset. The test MAEs of the MatPES PBE UMLIPs are close to the training and validation MAEs, indicating little or no overfitting. The test MAEs in energies of MPRelax and OMat24 UMLIPs are $> 4 - 10$ times higher than those of MatPES UMLIPs. It is not surprising that the MPRelax UMLIPs exhibit significantly higher energy errors due to the noise in the training data, as well as insufficient coverage of local environments far from equilibrium. Additionally, the exceptionally high energy error in the MPtrj CHGNet model stems from the inclusion of both PBE and PBE+ U calculations in its training data. The larger energy errors on the TensorNet OMat24 UMLIP is likely due to the lack of coverage of near-equilibrium local environments in OMat24. Furthermore, the TensorNet MatPES PBE UMLIP also exhibits generally uniform MAEs across all elements, while that trained on the TensorNet OMat24 UMLIP exhibits much higher errors on the rare earths and oxygen (Fig. S9).

Property benchmarks

To evaluate UMLIPs with different architectures and/or training data, we developed a set of equilibrium (relaxed structure similarity, formation energy), near-equilibrium (bulk and shear moduli, constant-volume heat capacity, force softening) and molecular dynamics (stability, ionic conductivity, efficiency) property benchmarks, collectively referred to as MatCalc³⁰-Bench. To ensure unbiased evaluation of UMLIPs trained with different datasets, the benchmark test data were curated from independent sources, including the Materials Project,^{5,31} Alexandria,³² WBM,³³ Graph Networks for Materials Science (GNoME),²² WBM high energy states,²¹ Materials Virtual Lab databases, summarized in Tab. S4.

Equilibrium benchmarks

As shown in Fig. 3, MatPES UMLIPs generally outperform MPRelax UMLIPs of the same architecture for equilibrium properties such as structural relaxations, but predict formation energies with comparable or slightly lower accuracy. Structures relaxed using MatPES PBE UMLIPs tend to have a lower mean “fingerprint” distance (defined in “Methods”) from DFT-PBE relaxed structures and with a lower variance than those relaxed using MPRelax UMLIPs. The MAE in formation energy per atom for the MatPES-trained M3GNet UMLIP is slightly higher than that of the MPF-trained M3GNet UMLIP. The MatPES CHGNet UMLIP, however, performs better than the MPtrj CHGNet UMLIP. We believe this is because the CHGNet model used here has a much higher model complexity (2,700,000 parameters) than the M3GNet model (664,000 parameters) and thus is able to better learn the diverse PES landscape of the dataset. The equivariant TensorNet models are able to achieve slightly lower fingerprint distance and formation energy errors than the invariant M3GNet and CHGNet models, despite having a relatively small number of parameters (838,000). The performance of MatPES r²SCAN UMLIPs is also generally excellent and similar to MatPES PBE UMLIPs.

Near-equilibrium benchmarks

The evaluation of UMLIPs on near-equilibrium properties was carried out primarily on MatPES PBE trained UMLIPs due to the lack of large r²SCAN datasets in the literature. Compared to MPRelax and OMat24 UMLIPs, we find that MatPES UMLIPs generally yield significant improvements in the prediction of the shear modulus G_{VRH} and off-equilibrium forces $|\mathbf{F}_i|$, while having similar performance in the prediction of the bulk modulus K_{VRH} and constant-volume heat capacity C_V (Fig. 4). The slightly better performance of MPRelax UMLIPs on K_{VRH} is expected due to the inclusion of a greater fraction of near-equilibrium relaxation structures in the dataset. The TensorNet-OMat24 UMLIP provides the most accurate predictions of C_V , probably due to the inclusion of numerous rattled configura-

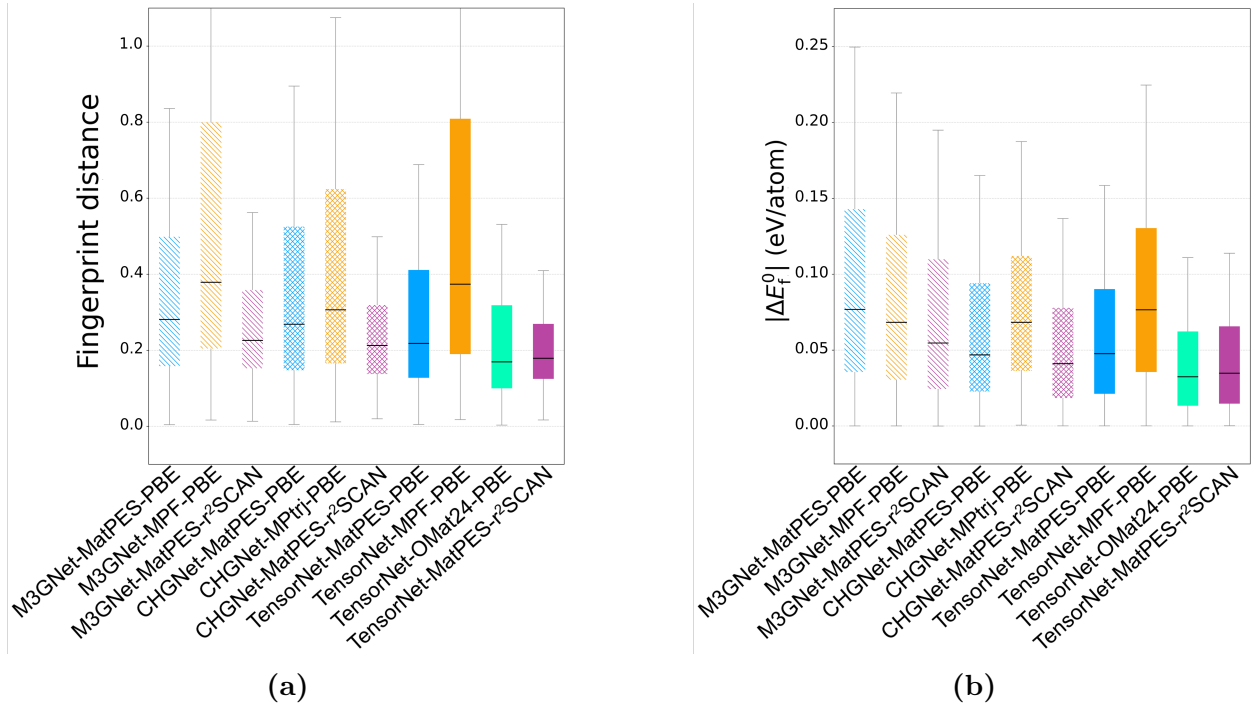


Fig. 3: Evaluation of UMLIPs on equilibrium properties. Distribution of the **a**, structural similarity fingerprint distance and **b**, formation energy per atom error between UMLIP and DFT-relaxed structures with the PBE and r²SCAN functionals. A random direction perturbation was applied to all sites of 1,000 out-of-domain PBE-relaxed and r²SCAN-relaxed structures randomly sampled from the WBM³³ and GNoME²² databases, respectively, prior to geometry optimization using UMLIPs. CrystalNN³⁴ was used to compute the fingerprint distance (see Methods).

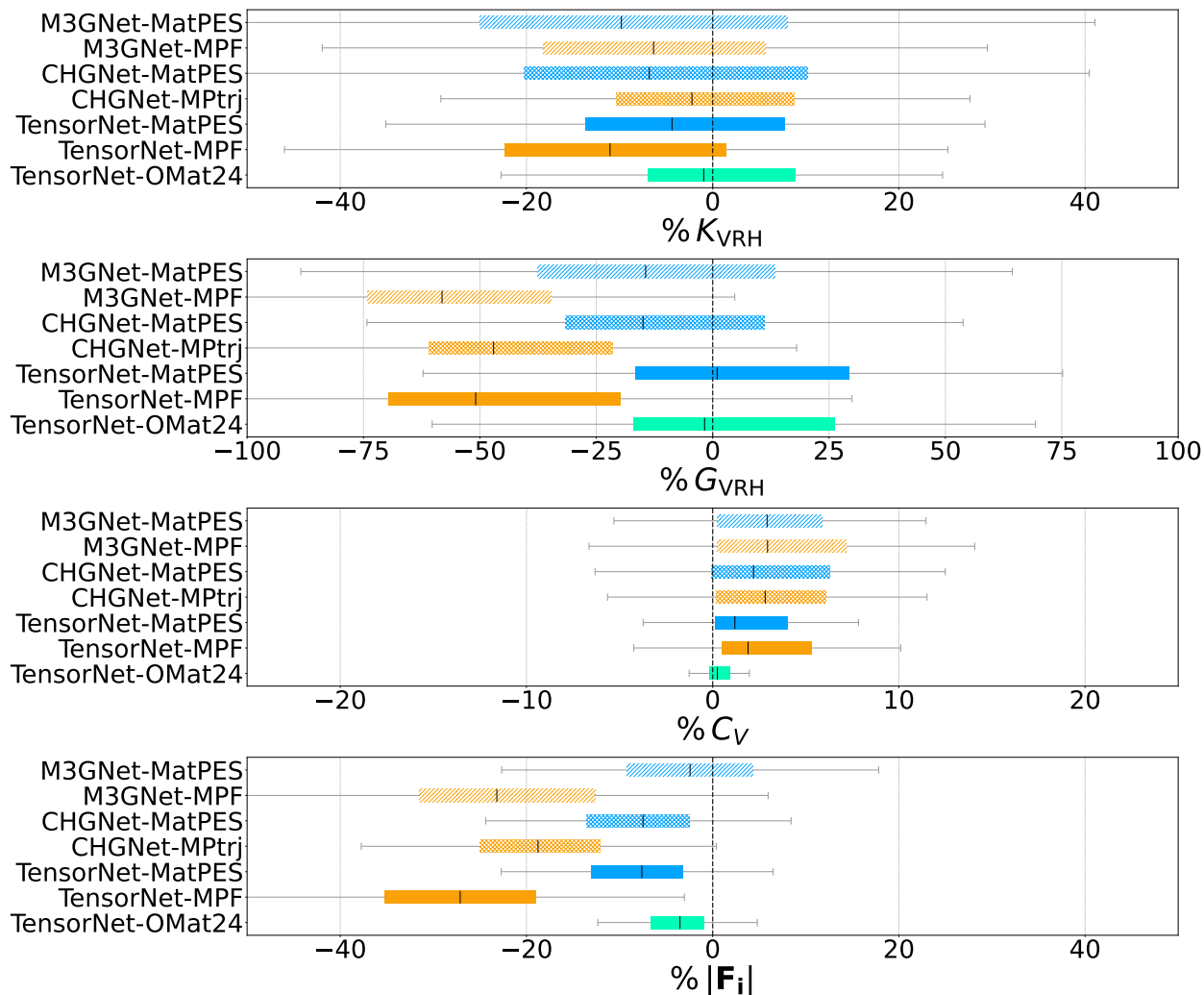


Fig. 4: Evaluation of UMLIPs on near-equilibrium properties. Distribution of the percentage errors in the predicted **a**, bulk moduli (K_{VRH}), **b**, shear moduli (G_{VRH}), **c**, constant-volume heat capacities (C_V), and **d**, off-equilibrium forces ($|\mathbf{F}_i|$) of MatPES PBE, MPRelax and OMat24 UMLIPs compared to the DFT ground truth. The elastic moduli benchmarks comprises 3,959 binary compounds with computed elastic moduli in the Materials Project.^{5,31} The C_V benchmark is derived within the harmonic approximation using 1,170 structures from the Alexandria phonon database.³² The $|\mathbf{F}_i|$ benchmark is computed from all 979 configurations in the WBM high energy states database.³³

tions through Boltzmann sampling. MatPES UMLIPs largely correct the systematic under-prediction of the PES curvature by MPRelax UMLIPs.²¹ We believe the remanent small systematic under-estimation of PES curvatures by MatPES UMLIPs will be addressed with the addition of structures from higher-temperature MD simulations in future MatPES dataset releases.

Molecular dynamics benchmarks

A primary application of UMLIPs is in MD simulations, but most existing benchmarks often do not include an assessment of UMLIP performance on MD stability or properties due to the lack of reference ab initio data. Here, a database of AIMD simulations of 172 battery materials performed by the Materials Virtual Lab over the past decade (MVL-batt) is used to evaluate UMLIPs.

A basic requirement for MD simulations is stability, which we assessed using the median termination temperature $T_{1/2}^{\text{term}}$ of 300 K-2,100 K linear heating MD simulations of the MVL-batt test structures (Fig. 5a). Common causes of terminations in MD simulations are volume explosion and atom loss. Given the same architecture, MatPES PBE UMLIPs exhibit significantly better MD stability, i.e., much larger $T_{1/2}^{\text{term}}$, compared to MPRelax and OMat24 UMLIPs. By 1500 K, less than 10% of the TensorNet-MatPES-PBE and TensorNet-MatPES-r²SCAN simulations have terminated, while about 55% and 65% of TensorNet-OMat24-PBE and TensorNet-MPF-PBE simulations, respectively, have terminated. Equivariant TensorNet UMLIPs generally exhibit better stability than invariant M3GNet UMLIPs. Also, MatPES r²SCAN UMLIPs exhibit better stability than MatPES PBE UMLIPs, which is likely due to the improved description of interatomic bonding by the r²SCAN functional.

The TensorNet-MatPES UMLIP significantly outperforms the TensorNet-MPF UMLIP (Fig. 5b) in terms of the predicted ionic conductivities (σ_{MLIP}). TensorNet-MPF UMLIP significantly overestimates σ_{MLIP} and has large errors spanning orders of magnitude (negative R^2). Again, this is likely due to the lack of off-equilibrium structures in the MPF dataset.

The performance of the TensorNet-OMat24 UMLIP is comparable to that of the TensorNet-MatPES UMLIP, but with a training data size that is 250 times larger.

Discussion

In recent years, advances in UMLIPs have been driven by ever larger models with increasing numbers of parameters, with the most performant models trained on closed source industry datasets, and evaluated on a narrow set of properties, mainly formation energies and stability classification.¹⁶ We believe that this trend presents significant risks. Reliance on large, proprietary datasets exacerbates reproducibility challenges and creates barriers that limit wider scientific participation. For instance, the training time for TensorNet on the MatPES-PBE dataset ($\sim 400,000$ structures) is about 15 minutes per epoch on a single Nvidia RTX A6000 GPU, while that for the same model on the OMat24 dataset (~ 100 million structures) is around 20 hours per epoch with sixteen Nvidia A100 GPUs. Furthermore, larger models require greater computational resources to run, restricting their feasibility for large-scale simulations (Tab. S5). The overemphasis on formation energies and stability classification overlooks other critical material properties essential for real-world applications.

Our findings challenge the notion that larger is always better for PES datasets. UMLIPs trained on the well-sampled MatPES dataset ($\sim 400,000$ structures) perform as well as or better than those trained on much larger datasets, such as MPtrj (~ 1 million structures) and OMat24 (~ 100 million structures). By introducing the first r²SCAN dataset that spans the periodic table, we also address a critical gap in PES descriptions from higher-order DFT methods. Finally, the MatCalc benchmark³⁰ provides a comprehensive evaluation of UMLIPs across a wide range of PES-derived properties.

This dataset release marks the beginning of the MatPES initiative. There is undoubtedly room to further expand the MatPES dataset beyond 300 K MD-sampled crystals, for example, by incorporating higher-temperature/pressure MD snapshots, defect structures,

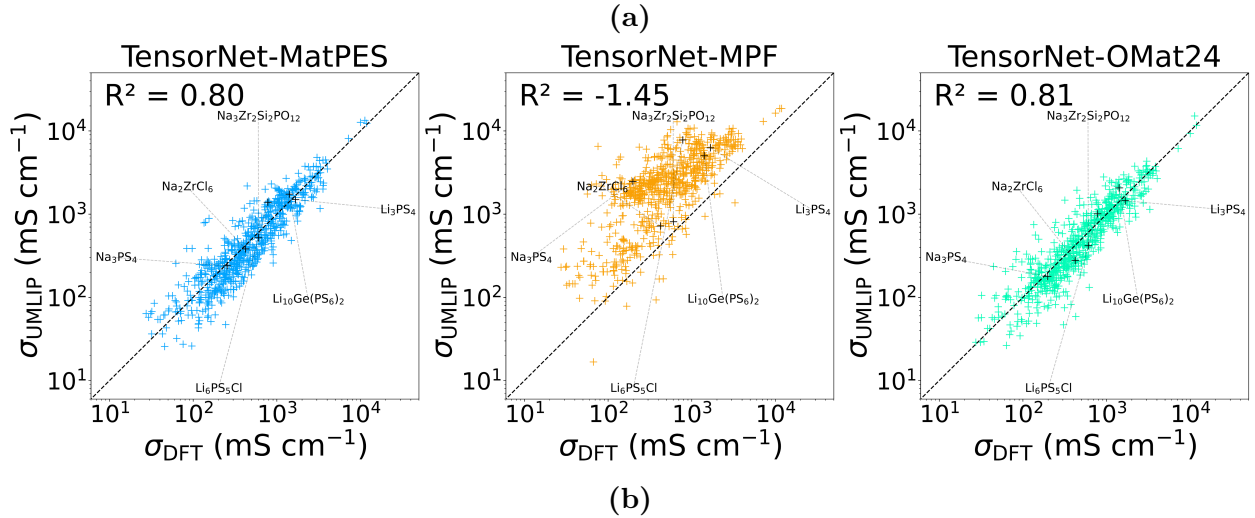
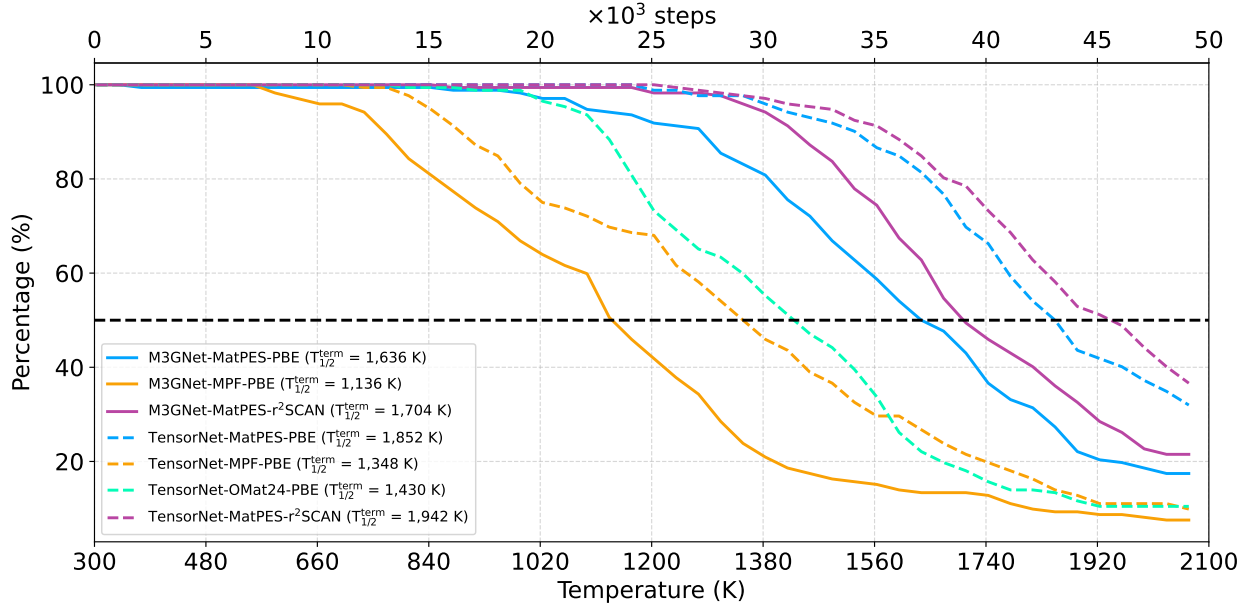


Fig. 5: Evaluation of UMLIPs on molecular dynamics (MD) properties of the MVL-Batt test set of 172 Li and Na-containing battery materials. **a**, Distributions of the MD termination steps of UMLIPs based a controlled heating protocol from 300 K to 2,100 K at 1 bar over 50 ps with a 1 fs time step for the MVL-Batt test set. Simulations terminate due to volume expansion ($V_t \geq 1.5V_0$) or atom loss. Three runs were performed per model for statistical reliability. Only the M3GNet and TensorNet architectures were used for these simulations. The metric to assess MD stability is the median termination temperature $T_{1/2}^{term}$, indicated for each of the UMLIPs in the legend. **b**, Parity plots of the UMLIP-predicted (σ_{MLIP}) against the AIMD (σ_{DFT}) Li/Na ionic conductivities of the MVL-Batt test set. A total of 698 *NVT* MD simulations at multiple temperatures (300-2,100 K) were performed. The data points for six well-known Li and Na solid electrolyte materials at 1,000 K are labeled for reference. The R^2 score is calculated from the mean squared error in $\log(\sigma)$ to ensure a robust evaluation across multiple orders of magnitude.

hypothetical materials, surfaces and interfaces, transition states, etc. The 2DIRECT workflow developed in this work provides a robust approach to these potential augmentation efforts in a data-efficient manner. We anticipate that these efforts will further enhance the reliability and accuracy of UMLIPs across diverse applications, solidifying their role as a cornerstone for materials discovery and design.

Methods

Configuration space generation and sampling

Of the 154,718 ground-state structures in Materials Project (v2022.10.28), a total of 151,768 structures with < 250 atoms in the unit cell were selected. For each structure, supercells were constructed so that the minimum distance between periodic neighbors is more than 7.5 \AA . Excluding supercells with more than 250 atoms and duplicates, the final set of initial structures totals 281,572. NpT MD simulations were then performed on these initial structures for 50,000 time steps at 300 K and 1 atm with the pre-trained M3GNet-MP-2021.2.8-DIRECT UMLIP²⁰ implemented in the Materials Graph Library (MatGL)²⁹ and Large-scale Atomic/Molecular Massively Parallel Simulator (LAMMPS).³⁵ The MD time interval was set to 2 fs and 0.5 fs for structures without and with hydrogen, respectively. In each MD run, 1,001 structures were dumped, resulting in 281,853,572 MD snapshot structures.

The M3GNet formation energy model¹ was used to encode the 281 million MD structures and their >16 billion atomic environments. The structural and atomic features had dimensionalities of 128 and 64, respectively. First, the 281 million structures were clustered into 15,192 clusters according to their locations in the structural feature space. Here, the first 16 PCs were used as structural features, as determined by Kaiser’s rule.²⁰ The threshold of BIRCH clustering was set to 0.5, as determined by memory limitations. Second, in each cluster, BIRCH clustering was performed in the atomic feature space with a threshold of 0.1. Normalization and dimensionality reduction were carried out to transform the 64-D M3GNet

atomic features to 8-D vectors. The scaler and PCA were fitted to the atomic features of the 154,718 ground-state structures only, as fitting them directly with the 16 billion atomic features is untractable. Finally, the structure with the smallest number of atoms in each cluster was selected to minimize DFT computational costs.

Density functional theory calculations

The MatPES training data were obtained from single-point (static) calculations using the Vienna *ab initio* Simulation Package (VASP)^{36–39} version 6.4.x. The VASP input parameters were carefully benchmarked for energy and force convergence and implemented as a “MatPESStaticSet” class in the open-source Python Materials Genomics (`pymatgen`) library,⁴⁰ versions 2025.1.9 and newer. The public availability of “MatPESStaticSet” allows users to generate additional training data to fine-tune MLIPs in a consistent manner. Tables S6 and S7 provide MatPES-compatible `INCAR` (including k -point density) and `POTCAR` settings, respectively. For large-scale data generation, the `MatPESStaticFlowMaker` function in the `atomate2` workflow orchestration package⁴¹ can be used.

Both the Perdew-Burke-Ernzerhof (PBE)¹⁷ generalized gradient approximation (GGA) and r²SCAN meta-GGA⁷ were employed to approximate the exchange-correlation energy. The self-consistent PBE orbitals were used as initial orbitals to accelerate r²SCAN calculations, useful for structures, which are far from equilibrium or with challenging bond arrangements. The most recent “PBE 64” pseudopotential library from VASP based on PBE all-electron calculations was used, and Gaussian Fermi surface broadening was used to ensure that interatomic forces in metals do not suffer from known errors in the tetrahedron method.⁴² Because Gaussian smearing contributes a small error to the total energy and forces via the electronic pseudo-entropy,⁴² we have ensured that the pseudo-entropy term contributes less than 1 meV atom⁻¹ to the total free energy by improving the “LargeSigmaHandler” in the `custodian` python package. This handler dynamically checks the pseudo-entropy term during a VASP calculation, and decreases the width of Fermi surface

broadening if the pseudo-entropy exceeds 1 meV/atom. The total DFT energy extrapolated to zero electronic smearing, the interatomic (Hellmann-Feynman) forces, and symmetric stress tensor were then used to train MLIPs. The lower success rate of the r²SCAN (77%) compared to the PBE (86%) calculations is consistent with the lower stability and higher cost of the r²SCAN functional.^{26,43} A fixed amount of computational resources was allocated to this project. Thus, the definition of “successful” calculations are those that ran within the budgeted computational resources *and* that converged, while “failed” calculations either did not complete within budgeted resources *or* did not converge.

UMLIP training

All ULIPs were trained using the MatGL package,²⁹ version 1.13. The key training hyperparameters are summarized in Table 2. All other hyperparameters were set to their default values. The total learnable parameters of M3GNet,¹ TensorNet,¹⁴ and CHGNet² are 664,000, 838,000, and 2,700,000, respectively.

Table 2: Training hyperparameters for UMLIPs

Parameter	M3GNet	TensorNet	CHGNet
Loss function	L_1	L_1	Huber with $\delta = 0.1$
Energy weight	1.0	1.0	1.0
Force weight	1.0	1.0	1.0
Stress weight	0.1	0.1	0.05
Magmom weight	N.A.	N.A.	1.0
Optimizer	AMSGrad AdamW ⁴⁴	AMSGrad AdamW ⁴⁴	Adam ⁴⁵
Initial learning rate	10^{-3}	10^{-3}	10^{-3}
Min. learning rate	10^{-5}	10^{-5}	10^{-5}
Bond distance cutoff	5 Å	5 Å	6 Å
Three-body cutoff	4 Å	N.A.	3 Å
Number of hidden neurons	128	128	128
Number of graph convolution layers	3	2	5
Basis expansion order	<code>max_n = 3, max_l = 3</code>	<code>max_n = 3</code>	<code>max_n = 63, max_f = 32</code>

Benchmarking metrics

Structure optimization

We randomly selected 1,000 structures relaxed with PBE from the WBM database³³ and 1,000 relaxed with r²SCAN from the MP recompute of the GNoME materials.²² Random atomic displacements of 0.1 Å were applied to these structures and then UMLIPs were used to relax the perturbed structures with the FIRE optimizer⁴⁶ and a 0.05 eV/Å force convergence criterion. The CrystalNN method³⁴ was used to compute the “fingerprint” vector of a structure based on its local environments. The similarity of a UMLIP-relaxed structure to its reference DFT-relaxed structure is then the Euclidean distance between their corresponding fingerprint vectors, with a lower distance indicating greater similarity between structures.

Cohesive and formation energy

The cohesive energy E_{coh} of a solid is defined as its total energy E_{solid} relative to its atomic (gas phase), E_i^{atom} , constituents with stoichiometric coefficients N_i ,

$$E_{\text{coh}} = \frac{1}{\sum_i N_i} \left[E_{\text{solid}} - \sum_i N_i E_i^{\text{atom}} \right]. \quad (1)$$

The formation energy of a solid at 0 K, E_f^0 , is defined as its total energy, E_{solid} , relative to the stoichiometry-weighted energies of the 0K ground state (solid phase) of its elemental constituents, E_i :

$$E_f^0 = \frac{1}{\sum_i N_i} \left[E_{\text{solid}} - \sum_i N_i E_i \right]. \quad (2)$$

Both the cohesive and formation energies are normalized by the number of atoms in the structure.

Elastic moduli and heat capacity

The bulk (K_{VRH}) and shear (G_{VRH}) moduli were extracted from the elastic tensor \mathbf{C} using the Voigt-Reuss-Hill (VRH) averaging scheme.⁴⁷

We selected the 3,959 binary structures from the Materials Project^{5,31} with converged PBE elastic tensors. These structures were relaxed using UMLIPs and then subjected to a series of normal and shear deformations to determine these constants. Linear strain values of $(-0.01, -0.005, 0.005, 0.01)$ and $(-0.06, -0.03, 0.03, 0.06)$ were used for each normal and shear modes, respectively. Shear deformation generally induced a weaker elastic response compared to normal deformation, so larger strains were required to ensure an accurate stress-strain fit.

The constant-volume heat capacity C_V is obtained from the partial derivative of the vibrational internal energy U_{vib} with respect to temperature under the harmonic phonon approximation:

$$C_V(T) = \left(\frac{\partial U_{\text{vib}}(T)}{\partial T} \right)_V. \quad (3)$$

Here, we focused on the heat capacity at room temperature ($T = 300$ K). As references, all 1,170 binary materials with converged PBE calculations in the Alexandria phonon database,³² were collected and relaxed by UMLIPs. A $2 \times 2 \times 2$ supercell was generated for each UMLIP-relaxed structure and an atomic displacement of 0.015 \AA was introduced into the supercell. Subsequently, the interatomic forces were calculated using UMLIPs for each supercell with displacement. The force constants were then obtained from the displacements and forces.

The dynamical matrix was constructed for each phonon wave vector \mathbf{q} in the Brillouin zone using the force constants obtained previously. The matrix was then diagonalized to obtain the phonon frequencies $\omega(\mathbf{q}\nu)$ and their corresponding eigenvectors. The Brillouin zone was sampled using a Γ -centered mesh with density proportional to the reciprocal lattice vector, scaled by 100. For each q -point, all phonon modes were calculated and the resulting

frequencies $\omega(\mathbf{q}\nu)$ were used to calculate U_{vib} at a given temperature T as

$$U_{\text{vib}}(T) = \sum_{\mathbf{q}\nu} \hbar \omega(\mathbf{q}\nu) \left\{ \frac{1}{2} + \left[\exp\left(\frac{\hbar \omega(\mathbf{q}\nu)}{k_{\text{B}} T}\right) - 1 \right]^{-1} \right\}, \quad (4)$$

where k_{B} and \hbar denote the Boltzmann constant and the reduced Planck constant, respectively.

MD benchmarks

The MD stability of a UMLIP is assessed using the median time-step of failure in a heating MD simulation in LAMMPS. A database of AIMD simulations of 172 battery materials performed by the Materials Virtual Lab over the past decade (MVL-batt) was used. Each material was relaxed and then heated from 300 K to 2,100 K at 1 bar over 50,000 time steps of 1 fs (50 ps in total). The final timestep at which the simulation crashed, due to explosion of the cell ($V_t \geq 1.5V_0$) or loss of atoms, was recorded for each material. Three runs were carried out for each material under the same conditions.

To compute the ionic conductivity, NVT MD simulations were performed using DFT and UMLIPs. A total of 698 simulations were carried out across a temperature range from 300 K to 2,100 K for the MVL-batt materials. Each simulation was run for at least 110 ps. The first 10 ps of the simulation were for equilibration, and the remaining 100 ps was used to compute the mean square displacement (MSD) of the diffusing species. The ionic conductivity σ is derived from the Nernst-Einstein equation:

$$\sigma = \frac{z^2 F^2 \rho}{RT} D, \quad (5)$$

where D is the diffusivity, ρ is the number density of diffusing ions, T is the absolute temperature, z is the ionic charge of the diffusing species ($z = 1$), F is Faraday's constant, and R is the universal gas constant. D is obtained from a linear fit of the MSD versus time, according to the Einstein relation:

$$D = \lim_{\Delta t \rightarrow \infty} \frac{1}{2d\Delta t} \left\langle |\mathbf{r}_i(t + \Delta t) - \mathbf{r}_i(t)|^2 \right\rangle_{i,t}, \quad (6)$$

where Δt denotes the time interval over which the particle displacement is measured and $\mathbf{r}_i(t + \Delta t)$ represents the position vector of the i^{th} diffusing ion at time $t + \Delta t$. $d = 3$ is the dimensionality of the system, and $\langle \dots \rangle$ indicates an ensemble average over the diffusing ion and time.

Data Availability

The MatPES dataset, with associated metadata and usage guide, is available via the MatPES.ai website (<http://matpes.ai>). The dataset is also available on the MPContribs platform²⁸ at https://materialsproject-contribs.s3.amazonaws.com/index.html#MatPES_2025_1/ as a bulk download, and via the explorer at https://next-gen.materialsproject.org/contribs/projects/MatPES_2025_1.

Code Availability

All software used in this work are publicly available in open-source libraries. The UMLIP architectures are available in the Materials Graph Library (MatGL).²⁹ The MatCalc-Bench is implemented in the MatCalc library.³⁰ The DFT computation and analysis code are available in the pymatgen,⁴⁰ atomate2,⁴¹ and emmet-core libraries.

References

- (1) Chen, C.; Ong, S. P. A universal graph deep learning interatomic potential for the periodic table. *Nature Comput. Sci.* **2022**, 718–728.
- (2) Deng, B.; Zhong, P.; Jun, K.; Riebesell, J.; Han, K.; Bartel, C. J.; Ceder, G. CHGNet

- as a pretrained universal neural network potential for charge-informed atomistic modelling. *Nat. Mach. Intell* **2023**, *5*, 1031–1041.
- (3) Batatia, I. et al. A foundation model for atomistic materials chemistry. 2024; <https://arxiv.org/abs/2401.00096>.
- (4) Kohn, W.; Sham, L. J. Self-consistent equations including exchange and correlation. *Phys. Rev.* **1965**, *140*, A1133.
- (5) Jain, A.; Ong, S. P.; Hautier, G.; Chen, W.; Richards, W. D.; Dacek, S.; Cholia, S.; Gunter, D.; Skinner, D.; Ceder, G.; Persson, K. A. Commentary: The Materials Project: A materials genome approach to accelerating materials innovation. *APL Materials* **2013**, *1*, 011002.
- (6) Schmidt, J.; Hoffmann, N.; Wang, H.; Borlido, P.; Carriço, P. J. M. A.; Cerqueira, T. F. T.; Botti, S.; Marques, M. A. L. Machine-Learning-Assisted Determination of the Global Zero-Temperature Phase Diagram of Materials. *Advanced Materials* **2023**, *35*.
- (7) Furness, J. W.; Kaplan, A. D.; Ning, J.; Perdew, J. P.; Sun, J. Accurate and Numerically Efficient r²SCAN Meta-Generalized Gradient Approximation. *J. Phys. Chem. Lett.* **2020**, *11*, 8208–8215.
- (8) Lennard-Jones, J. E. Cohesion. *Proc. Phil. Soc.* **1931**, *43*, 461.
- (9) Daw, M. S.; Baskes, M. I. Embedded-atom method: Derivation and application to impurities, surfaces, and other defects in metals. *Phys. Rev. B* **1984**, *29*, 6443–6453.
- (10) Senftle, T. P.; Hong, S.; Islam, M. M.; Kylasa, S. B.; Zheng, Y.; Shin, Y. K.; Junkermeier, C.; Engel-Herbert, R.; Janik, M. J.; Aktulga, H. M.; Verstraelen, T.; Grama, A.; van Duin, A. C. T. The ReaxFF reactive force-field: development, applications and future directions. *npj Comput. Mater.* **2016**, *2*, 1–14.

- (11) Ko, T. W.; Ong, S. P. Recent advances and outstanding challenges for machine learning interatomic potentials. *Nat. Comput. Sci.* **2023**, *3*, 998–1000.
- (12) Zhang, Y.-W.; Sorkin, V.; Aitken, Z. H.; Politano, A.; Behler, J.; Thompson, A. P.; Ko, T. W.; Ong, S. P.; Chalykh, O.; Korogod, D.; others Roadmap for the development of machine learning-based interatomic potentials. *Modelling Sim. Mater. Sci. Engr.* **2025**, *33*, 023301.
- (13) Batatia, I.; Kovacs, D. P.; Simm, G.; Ortner, C.; Csanyi, G. MACE: Higher Order Equivariant Message Passing Neural Networks for Fast and Accurate Force Fields. *Advances in Neural Information Processing Systems*. 2022; pp 11423–11436.
- (14) Simeon, G.; Fabritiis, G. D. TensorNet: Cartesian Tensor Representations for Efficient Learning of Molecular Potentials. *Thirty-seventh Conference on Neural Information Processing Systems*. 2023.
- (15) Qiao, Z.; Welborn, M.; Anandkumar, A.; Manby, F. R.; Miller, I., Thomas F. OrbNet: Deep learning for quantum chemistry using symmetry-adapted atomic-orbital features. *J. Chem. Phys.* **2020**, *153*, 124111.
- (16) Riebesell, J.; Goodall, R. E. A.; Benner, P.; Chiang, Y.; Deng, B.; Ceder, G.; Asta, M.; Lee, A. A.; Jain, A.; Persson, K. A. Matbench Discovery – A framework to evaluate machine learning crystal stability predictions. 2024; <https://arxiv.org/abs/2308.14920>.
- (17) Perdew, J. P.; Burke, K.; Ernzerhof, M. Generalized gradient approximation made simple. *Phys. Rev. Lett.* **1996**, *77*, 3865.
- (18) Jain, A.; Hautier, G.; Ong, S. P.; Moore, C. J.; Fischer, C. C.; Persson, K. A.; Ceder, G. Formation enthalpies by mixing GGA and GGA + U calculations. *Phys. Rev. B* **2011**, *84*, 045115.

- (19) Shishkin, M.; Sato, H. DFT+U in Dudarev’s formulation with corrected interactions between the electrons with opposite spins: The form of Hamiltonian, calculation of forces, and bandgap adjustments. *J. Chem. Phys.* **2019**, *151*, 024102.
- (20) Qi, J.; Ko, T. W.; Wood, B. C.; Pham, T. A.; Ong, S. P. Robust Training of Machine Learning Interatomic Potentials with Dimensionality Reduction and Stratified Sampling. *npj Comput. Mater.* *10*, 43.
- (21) Deng, B.; Choi, Y.; Zhong, P.; Riebesell, J.; Anand, S.; Li, Z.; Jun, K.; Persson, K. A.; Ceder, G. Overcoming systematic softening in universal machine learning interatomic potentials by fine-tuning. 2024; <https://arxiv.org/abs/2405.07105>.
- (22) Merchant, A.; Batzner, S.; Schoenholz, S. S.; Aykol, M.; Cheon, G.; Cubuk, E. D. Scaling deep learning for materials discovery. *Nature* **2023**, *624*, 80–85.
- (23) Yang, H. et al. MatterSim: A Deep Learning Atomistic Model Across Elements, Temperatures and Pressures. 2024; <https://arxiv.org/abs/2405.04967>.
- (24) Barroso-Luque, L.; Shuaibi, M.; Fu, X.; Wood, B. M.; Dzamba, M.; Gao, M.; Rizvi, A.; Zitnick, C. L.; Ulissi, Z. W. Open Materials 2024 (OMat24) Inorganic Materials Dataset and Models. 2024; <https://arXiv:2410.12771>.
- (25) Tran, F.; Stelzl, J.; Blaha, P. Rungs 1 to 4 of DFT Jacob’s ladder: Extensive test on the lattice constant, bulk modulus, and cohesive energy of solids. *J. Chem. Phys.* **2016**, *144*, 204120.
- (26) Kingsbury, R.; Gupta, A. S.; Bartel, C. J.; Munro, J. M.; Dwaraknath, S.; Horton, M.; Persson, K. A. Performance comparison of r^2 SCAN and SCAN metaGGA density functionals for solid materials via an automated, high-throughput computational workflow. *Phys. Rev. Mater.* **2022**, *6*, 013801.

- (27) Kothakonda, M.; Kaplan, A. D.; Isaacs, E. B.; Bartel, C. J.; Furness, J. W.; Ning, J.; Wolverton, C.; Perdew, J. P.; Sun, J. Testing the r²SCAN Density Functional for the Thermodynamic Stability of Solids with and without a van der Waals Correction. *ACS Materials Au* **2023**, *3*, 102–111.
- (28) Huck, P.; Gunter, D.; Cholia, S.; Winston, D.; N’Diaye, A. T.; Persson, K. User applications driven by the community contribution framework MPContribs in the Materials Project. *Concurrency and Computation: Practice and Experience* **2016**, *28*, 1982–1993.
- (29) Ko, T. W.; Nassar, M.; Qi, J.; Miret, S.; Liu, E.; Deng, B.; Barroso-Luque, L.; Ong, S. P. MatGL: <https://github.com/materialsvirtuallab/matgl>.
- (30) Liu, R.; Liu, E.; Riebesell, J.; Qi, J.; Ong, S. P.; Ko, T. W. MatCalc: <https://github.com/materialsvirtuallab/matcalc>.
- (31) de Jong, M.; Chen, W.; Angsten, T.; Jain, A.; Notestine, R.; Gamst, A.; Sluiter, M.; Krishna Ande, C.; van der Zwaag, S.; Plata, J. J.; Toher, C.; Curtarolo, S.; Ceder, G.; Persson, K. A.; Asta, M. Charting the complete elastic properties of inorganic crystalline compounds. *Sci. Data* **2015**, *2*.
- (32) Loew, A.; Sun, D.; Wang, H.-C.; Botti, S.; Marques, M. A. L. Universa Machine Learning Interatomic Potentials are Ready for Phonons. 2024; <http://arxiv.org/abs/2412.16551>.
- (33) Wang, H.-C.; Botti, S.; Marques, M. A. L. Predicting stable crystalline compounds using chemical similarity. *npj Computational Materials* **2021**, *7*, 1–9.
- (34) Zimmermann, N. E. R.; Jain, A. Local structure order parameters and site fingerprints for quantification of coordination environment and crystal structure similarity. *RSC Adv.* **2020**, *10*, 6063–6081.

- (35) Thompson, A. P.; Aktulga, H. M.; Berger, R.; Bolintineanu, D. S.; Brown, W. M.; Crozier, P. S.; in 't Veld, P. J.; Kohlmeyer, A.; Moore, S. G.; Nguyen, T. D.; Shan, R.; Stevens, M. J.; Tranchida, J.; Trott, C.; Plimpton, S. J. LAMMPS - a flexible simulation tool for particle-based materials modeling at the atomic, meso, and continuum scales. *Comp. Phys. Comm.* **2022**, *271*, 108171.
- (36) Kresse, G.; Hafner, J. *Ab initio* molecular dynamics for liquid metals. *Physical Review B* **1993**, *47*, 558–561.
- (37) Kresse, G.; Hafner, J. *Ab initio* molecular-dynamics simulation of the liquid-metal–amorphous-semiconductor transition in germanium. *Physical Review B* **1994**, *49*, 14251–14269.
- (38) Kresse, G.; Furthmüller, J. Efficient iterative schemes for *ab initio* total-energy calculations using a plane-wave basis set. *Physical Review B* **1996**, *54*, 11169–11186.
- (39) Kresse, G.; Furthmüller, J. Efficiency of *ab-initio* total energy calculations for metals and semiconductors using a plane-wave basis set. *Computational Materials Science* **1996**, *6*, 15–50.
- (40) Ong, S. P.; Richards, W. D.; Jain, A.; Hautier, G.; Kocher, M.; Cholia, S.; Gunter, D.; Chevrier, V. L.; Persson, K. A.; Ceder, G. Python Materials Genomics (pymatgen): A robust, open-source python library for materials analysis. *Comput. Mater. Sci.* **2013**, *68*, 314–319.
- (41) Ganose, A. et al. Atomate2: Modular workflows for materials science. 2025; <http://dx.doi.org/10.26434/chemrxiv-2025-tcr5h>.
- (42) dos Santos, F. J.; Marzari, N. Fermi energy determination for advanced smearing techniques. *Phys. Rev. B* **2023**, *107*, 195122.

- (43) Mejía-Rodríguez, D.; Trickey, S. B. Meta-GGA performance in solids at almost GGA cost. *Phys. Rev. B* **2020**, *102*, 121109.
- (44) Loshchilov, I.; Hutter, F. Decoupled Weight Decay Regularization. 2019; <https://arxiv.org/abs/1711.05101>.
- (45) Kingma, D. P.; Ba, J. Adam: A Method for Stochastic Optimization. **2014**,
- (46) Bitzek, E.; Koskinen, P.; Gähler, F.; Moseler, M.; Gumbusch, P. Structural Relaxation Made Simple. *Phys. Rev. Lett.* **2006**, *97*, 170201.
- (47) Hill, R. The Elastic Behaviour of a Crystalline Aggregate. *Proc. Phys. Soc. A* **1952**, *65*, 349.

Acknowledgement

This work was intellectually led by the U.S. Department of Energy, Office of Science, Office of Basic Energy Sciences, Materials Sciences and Engineering Division under contract No. DE-AC02-05-CH11231 (Materials Project program KC23MP). This research used resources of the National Energy Research Scientific Computing Center (NERSC), a Department of Energy Office of Science User Facility using NERSC award DOE-ERCAP0026371. A portion of the research was performed using computational resources sponsored by the Department of Energy’s Office of Energy Efficiency and Renewable Energy and located at the National Renewable Energy Laboratory. A portion of the research used the Lawrence computational cluster resource provided by the IT Division at the Lawrence Berkeley National Laboratory (Supported by the Director, Office of Science, Office of Basic Energy Sciences, of the U.S. Department of Energy under Contract No. DE-AC02-05CH11231) T. W. Ko also acknowledges the support of the Eric and Wendy Schmidt AI in Science Postdoctoral Fellowship, a Schmidt Futures program. We acknowledge Xiaoxu Ruan for initial discussions regarding the `MatPESStaticSet`.

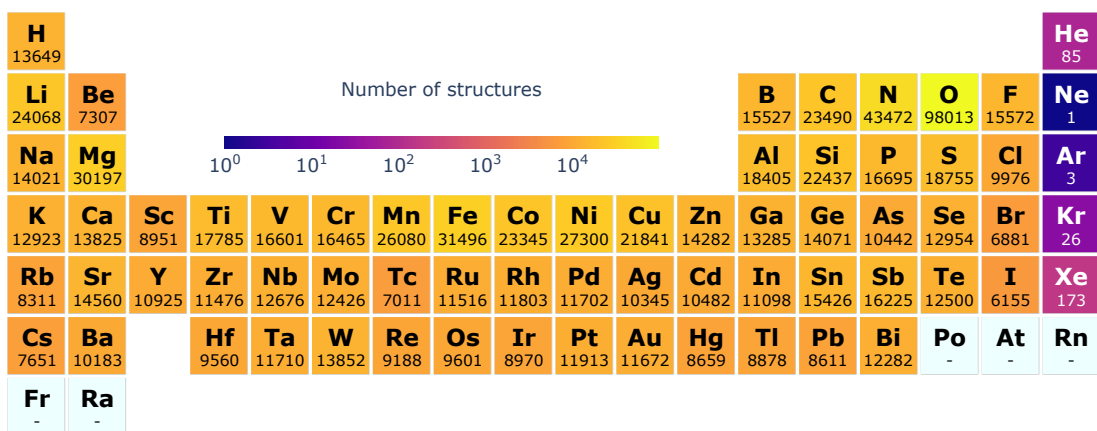
Author Contributions

A.D.K.: benchmarking and performing DFT calculations; revision of DFT workflows; selecting equilibrium structures to augment MD set from the Materials Project and to perform r²SCAN benchmarks from the MP-GNoME structures; writing and editing the manuscript; design of the MPContribs dataset. R.L.: design and implementation of the benchmarking workflows; performing the equilibrium properties, elastic moduli, constant-volume heat capacity and molecular dynamics properties benchmarks; collating the AIMD results; writing and editing the manuscript. J.Q.: project initiation and conception; design and execution of the configuration space expansion and 2DIRECT sampling; development of batched dataset loading in MatGL and training of TensorNet-OMat24; development of `MatPESStaticSet`; manuscript writing. T.W.K.: Training M3GNet and TensorNet models for both MPF and MatPES datasets; manuscript editing. B.D.: Training CHGNet; benchmarking force softening; manuscript editing. J.R.: conceptualization of sampling method; benchmarking of DFT parameters; implementation of `MatPESStaticSet`; writing workflows; manuscript editing. G.C.: manuscript editing; provision of computational resources. K.A.P.: project design; manuscript editing; provision of computational and data dissemination resources. S.P.O.: project design and conception; manuscript writing; provision of computational and data dissemination resources; `matpes.ai` website development.

Supplementary Information: A Foundational Potential Energy Surface Dataset for Materials

Table S3: Number of structures, mean (μ) and standard deviation (σ) of the cohesive energies E_{coh} , interatomic force magnitudes $|\mathbf{F}_i|$ and pressure for the different datasets. The MatPES PBE dataset has mean E_{coh} and $|\mathbf{F}_i|$ that are between those of the MPF/MPtrj and OMat24 datasets.

	Number	E_{coh} (eV/atom)		$ \mathbf{F}_i $ (eV/Å)		Pressure (GPa)		Ref
		μ	σ	μ	σ	μ	σ	
MPF	185,877	-4.273	2.035	0.527	4.440	-2.374	37.768	[1]
MPtrj	1,580,395	-4.325	1.254	0.327	1.361	0.281	6.217	[2]
OMat24	100,824,585	-4.610	2.000	1.970	4.630	2.403	9.613	[24]
MatPES PBE	434,712	-4.163	1.432	0.811	3.274	1.596	10.981	This work
MatPES r ² SCAN	387,897	-4.008	1.352	0.935	2.951	0.893	11.482	This work



La 11435	Ce 8434	Pr 3389	Nd 3766	Pm 997	Sm 3394	Eu 6277	Gd 3770	Tb 2326	Dy 2004	Ho 2141	Er 2104	Tm 2139	Yb 5148	Lu 3144
Ac 2526	Th 6507	Pa 4125	U 9141	Np 4785	Pu 7954	Am -	Cm -	Bk -	Cf -	Es -	Fm -	Md -	No -	Lr -

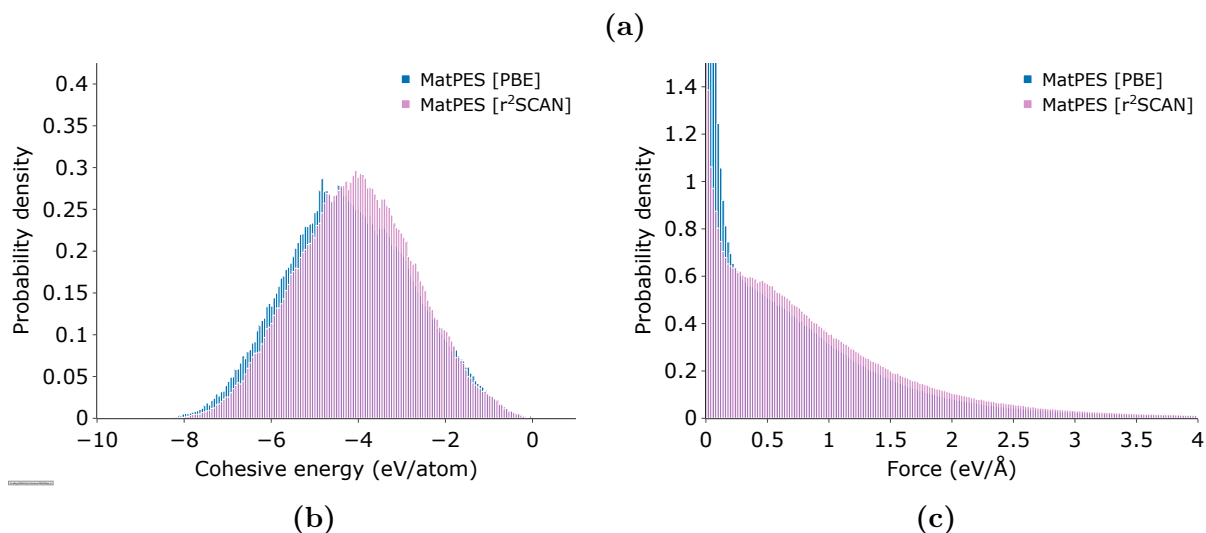


Fig. S6: Coverage of the MatPES r^2 SCAN dataset. **a**, Heat map of the element distribution in the MatPES r^2 SCAN dataset. The number in each cell is the number of structures in the MatPES r^2 SCAN dataset containing that element, plotted on a logarithmic scale. Distribution of **b**, cohesive energies (E_{coh}) and **c**, interatomic force magnitudes ($|\mathbf{F}_i|$) in the MatPES r^2 SCAN dataset (purple), with the PBE dataset (blue) plotted for comparison. The composition of the datasets are as follows: MatPES PBE: 434,712 structures (326,635 MD snapshots, 108,077 MP equilibrium structures); MatPES r^2 SCAN: 387,897 structures (302,373 MD snapshots, 85,524 MP equilibrium structures).

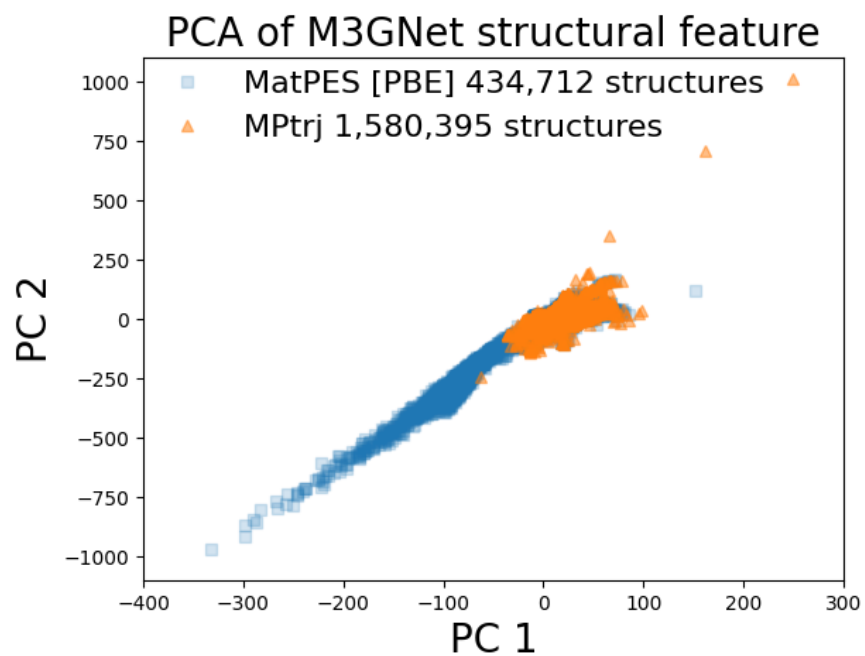


Fig. S7: Coverage of MatPES vs MPtrj datasets. Plot of the first two principal components of the structures in the MatPES and MPtrj datasets, using the principal component analysis trained on the structural features on all MD snapshots. It is clear that the MatPES dataset covers a much range in the PC space.

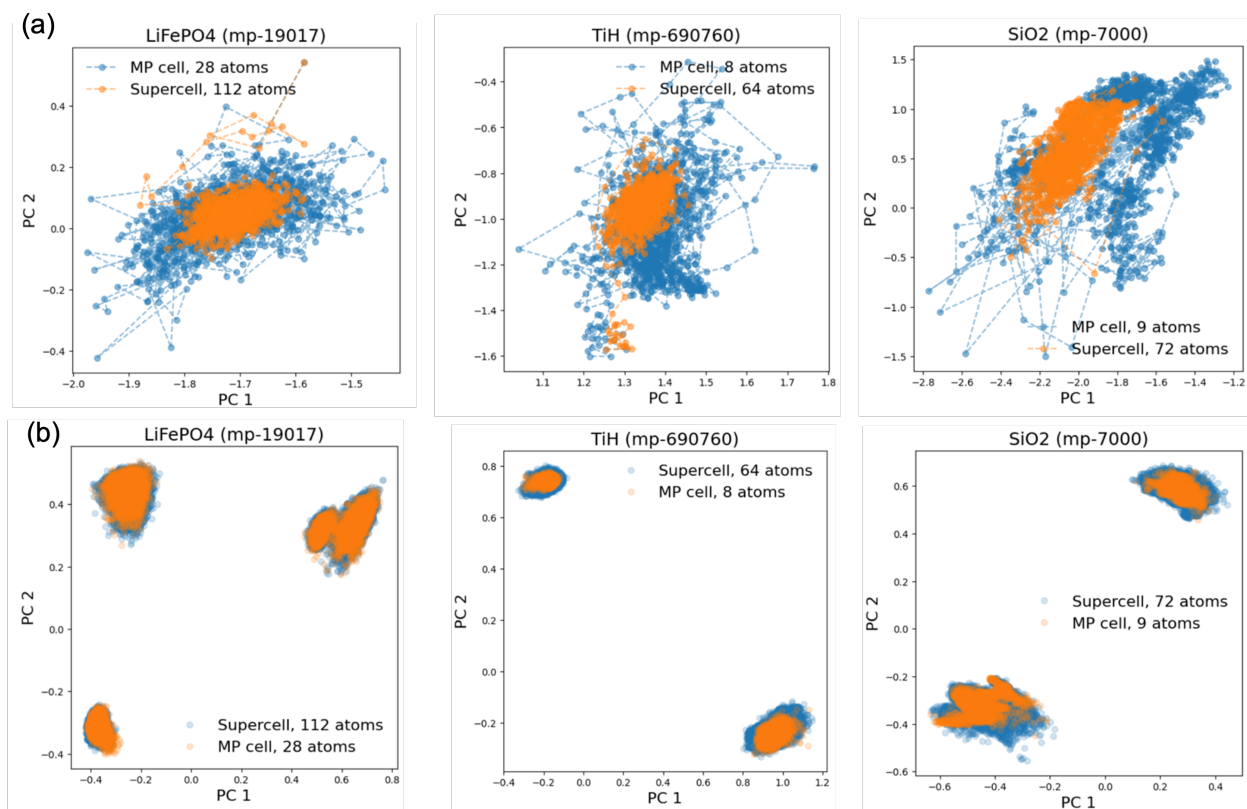
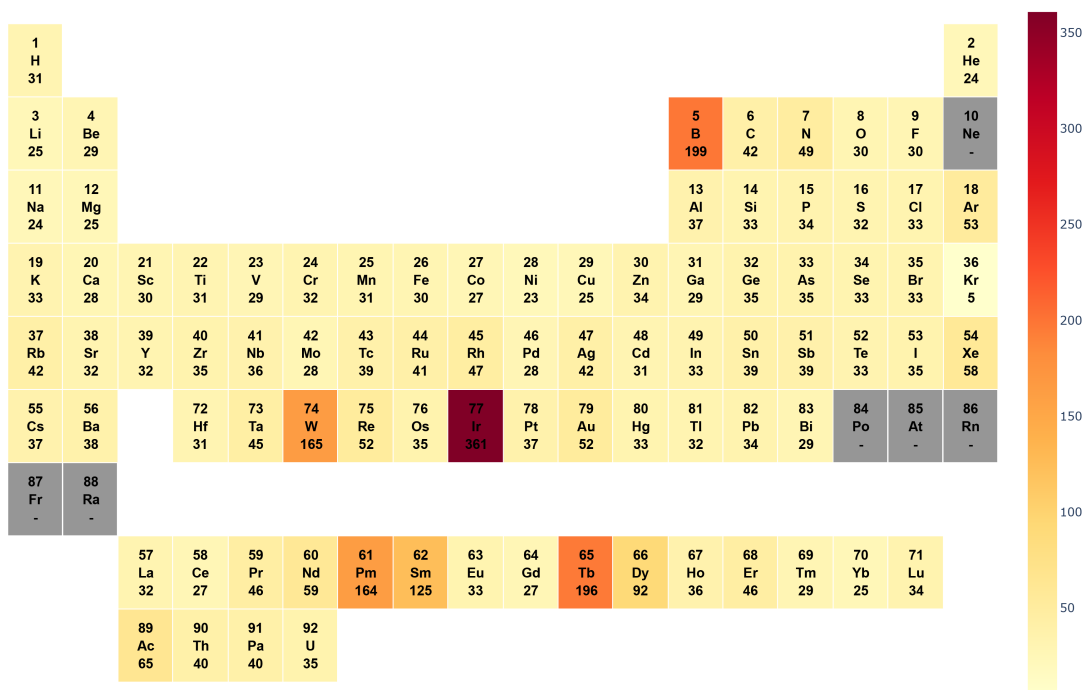
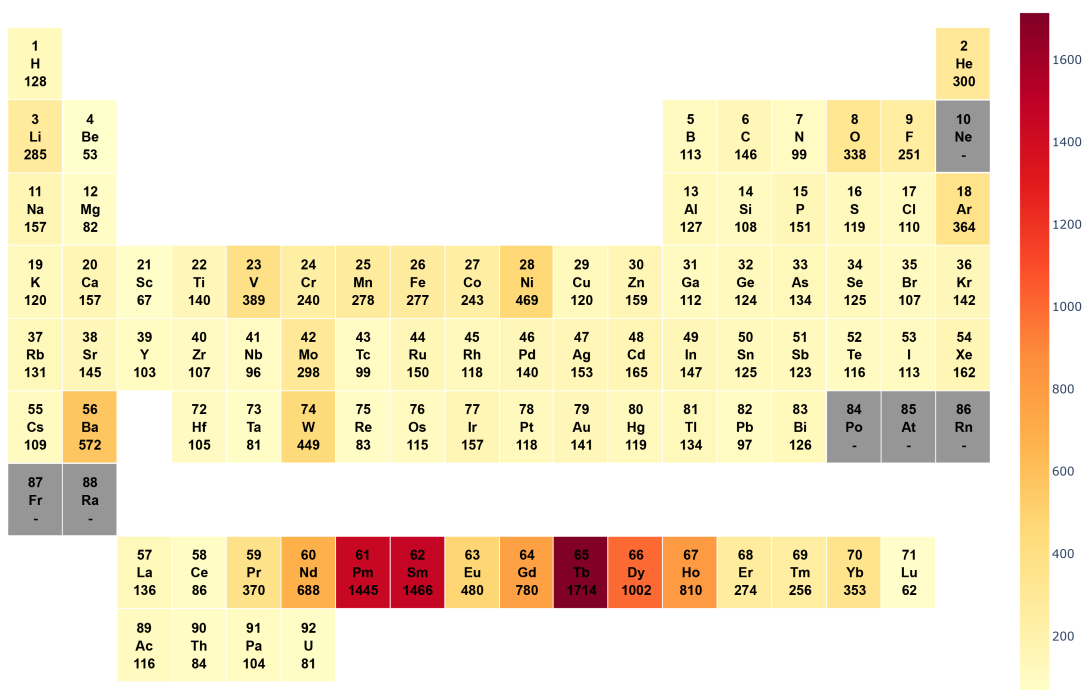


Fig. S8: Coverage of structural and atomic feature space by supercells and unit cells. Two dimensional principal component analysis (PCA) feature space of M3GNet for a, structural and b, atomic features sampled in 100 ps of NpT -MD at 300 K and 1 atm for three representative materials - LiFePO₄ (mp-19017), TiH₂ (mp-690760), and SiO₂ (mp-7000). The MD supercells cover a smaller region in structural feature space than the corresponding unit cells, due to the normalization over a larger number of atoms. However, the supercells cover a larger region in atomic feature space than the corresponding unit cells.



(a)



(b)

Fig. S9: Elemental heatmap of test mean absolute errors (MAEs) in energies. MAEs shown are for TensorNet UMLIPs trained on **a**, MatPES PBE and **b**, OMat24 datasets.

Table S4: Overview of MatCalc-Benchmark metrics. They can be divided into three categories: equilibrium, near-equilibrium, and molecular dynamics properties. The time per atom per time step t_{step} was computed using MD simulations conducted on a single Intel Xeon Gold core for a system of 64 Si atoms under ambient conditions (300 K and 1 bar) over 50 ps with a 1 fs time step. These properties were all computed using the MatCalc library.³⁰

Task	Functional	Test Data Source	Number
Equilibrium			
Structural similarity	PBE	WBM ³³	1,000
	r ² SCAN	GNoME ²²	1,000
Formation energy per atom (E_f^0)	PBE	WBM	1,000
	r ² SCAN	GNoME	1,000
Near-equilibrium			
Bulk modulus (K_{VRH})	PBE	MP ⁵	3,959
Shear modulus (G_{VRH})	PBE	MP	3,959
Const. vol. heat capacity (C_V)	PBE	Alexandria ³²	1,170
Off-equilibrium force ($ \mathbf{F}_i $)	PBE	WBM high energy states ²¹	979
Molecular dynamics			
Median termination temp ($T_{1/2}^{\text{term}}$)	PBE & r ² SCAN	This work	172
Ionic conductivity (σ)	PBE	This work	698
Time per atom per time step (t_{step})	PBE & r ² SCAN	This work	1

Table S5: Computational cost of different UMLIPs. The time per atom per time step was estimated from MD simulations conducted on a single Intel Xeon Gold core for a system of 64 Si atoms under ambient conditions (300 K and 1 bar) over 50 ps with a 1 fs time step. The total learnable parameters of the M3GNet, TensorNet, and CHGNet models used in this work are 664,000, 838,000, and 2,700,000, respectively. A clear correlation is seen between the computational cost and the number of model parameters.

UMLIP	Time (ms/atom/step)
MatPES PBE	
M3GNet	1.957
CHGNet	4.915
TensorNet	3.014
MatPES r²SCAN	
M3GNet	1.943
CHGNet	4.875
TensorNet	3.052
MPF	
M3GNet	2.095
TensorNet	1.803
MPtrj	
CHGNet	4.397
OMat24	
TensorNet	3.114

Table S6: VASP INCAR settings used for MatPES. For PBE¹⁷ calculations, the GGA tag was set to “PE”, and for r²SCAN⁷ calculations, the GGA tag was not set, and the METAGGA tag was set to “R2SCAN”.

Parameter	Value
ALGO	Normal
EDIFF	1e-05
ENAUG	1360
ENCUT	680
ISMEAR	0
ISPIN	2
KSPACING	0.22
LAECHG	True
LASPH	True
LCHARG	True
LDAU	False
LDAUTYPE	2
LMAXMIX	6
LMIXTAU	True
LORBIT	11
LREAL	False
LWAVE	False
NELM	200
NSW	0
PREC	Accurate
SIGMA	0.05

Table S7: VASP pseudopotentials (POTCAR) used for MatPES. The second column indicates the “TITEL” keyword of the POTCAR, and the third column indicates the SHA256 hash that is included in the POTCAR file. MatPES uses the “PBE 64” PAW pseudopotential library.

El.	TITEL	SHA
Ac	PAW_PBE Ac 06Sep2000	ef0c2b83cf569bea36d28252deb147ae18f4f417709a0a90a00fa0751e60408a
Ag	PAW_PBE Ag 02Apr2005	6550cfa3543261e132c169e1b98a529204624d72be14e2da2e0242bcb74a174d
Al	PAW_PBE Al 04Jan2001	17880443556af62b473fe41b62a467bd001ad55d2cabe504a3f22e34d4e9db96
Am	PAW_PBE Am 08May2007	ed4d25cb37bf36722bf7da53aff49a5f32f6e6cb278d4cb693f29442583ade28
Ar	PAW_PBE Ar 07Sep2000	94ccc759e5215f718956dfe5fb43b4f2f2ae700f97accfbf846e1c2491cbae56
As	PAW_PBE As 22Sep2009	bc8fb55b00baa90d383a523722e1771deb40ea3f17a5ce25913641995975acad
At	PAW_PBE At 21May2007	324a31b576a03b2f68d883a08822bc631d1aee72d359804fa17db26f45fb52bb
Au	PAW_PBE Au 04Oct2007	d0044ae04e2bdce24051b198fc5c053d722a5bc6fe3c3b100514a13fc5d2db88
B	PAW_PBE B 06Sep2000	a32ced30f5ae56fd4d10b4325ff17eb3e4e38ee0f4288bc219fb012fddfa6e97
Ba	PAW_PBE Ba_sv_GW 30Nov2021	729cfb57c5620ba7c0f6e42203de8340b45f71b59c373a5821ca22f69225df8c
Be	PAW_PBE Be_sv 06Sep2000	95d73059eaf0de9a2d42225277cca956d5b2c38504d1b500b1a4c08b9931b7a
Bi	PAW_PBE Bi 08Apr2002	d6b6753ed5db3f0e277fb15e6dbb6699c4bc829850a481068e9e7236faeca489
Br	PAW_PBE Br 06Sep2000	96a73d2954943bbee26f4990d676cc6c3bf44b8dd2c75cd4b3b825d8403f0103
C	PAW_PBE C 08Apr2002	253f7b50bb8d59471dbedb8285d89021f4a42ed1a2c5d38a03a736e69125dd95
Ca	PAW_PBE Ca_sv 06Sep2000	a47365830e737f14e0e6c5cf1ed81b94e081eecf0a33df105380881bc9da05d5
Cd	PAW_PBE Cd 06Sep2000	8b7ca71966beae5276c8bb910adb3ecc013a3354c27473914c94cd54c83be4f7

El.	TITEL	SHA
Ce	PAW_PBE Ce 23Dec2003	00bd3101dba980d69718c826e9aff48526de61f93249f80fb0d1cde9afca69b7
Cf	PAW_PBE Cf 17Oct2013	9d2a2d228fc4747daad0b17273e4831741ec188f58739a971ab0474c5ff36db3
Cl	PAW_PBE Cl 06Sep2000	9f1b6e6ed4247ac726a768b330d26d7667cc3c95a39ff49c1d064c2d9dce931
Cm	PAW_PBE Cm 17Jan2011	10f7147aec31bdfcd023378638ce6d89b1eef3e653eb06887ddc6b577c1a20c8
Co	PAW_PBE Co 02Aug2007	0e690c60710354995174544f52f9f2c30879afabeffe3b3fbd4001cb294e56d4
Cr	PAW_PBE Cr_pv 02Aug2007	c9a7df34d3cdbacf1090e328ef39c0b420964e11c23f63548d1ac9dd218cdba0
Cs	PAW_PBE Cs_sv 25Jan2019	0e16bce67778f8d3e6a1e8d49098acae95c0f8d441dd09aee70633bcf454619d
Cu	PAW_PBE Cu_pv 06Sep2000	cb7b504e2ea725fe1f25c85a9ac77d4012ce94cd394135b722c4e25ec297f1cb
Dy	PAW_PBE Dy_h 30May2022	22476d747c0ad3010bbc2b9b82ce7b879d05e04135e746a70820417bee947c38
Er	PAW_PBE Er_h 29Jun2022	2b80424db8faabd5254b489548b03ac32ffe345d20d95add1e30ba732b45f18a
Eu	PAW_PBE Eu 25May2022	60d5a46ff9a0a7f4ab06309e7661032aad63da4a27607063648b9a9b69393f0f
F	PAW_PBE F 08Apr2002	53c630871ac675939349fc2b976745ee17808dedc90b5bdde026bc81f0faf456
Fe	PAW_PBE Fe_pv 02Aug2007	5d22e414b1f82158bf2c7ecb8b97b28fd0923e48cad1c3bf74d524558f5dd32
Fr	PAW_PBE Fr_sv 29May2007	23d9c34aa2eb6adab1bca1262c635f9251f4b1fe31f8522b3106ee5dd2f6057e
Ga	PAW_PBE Ga_d 06Jul2010	a60ddf36e14f00ea098d9e3914b3745f1b7105e68786148f49ae384e44b4226c
Gd	PAW_PBE Gd 25May2022	b942d524b9340ee44669b7c5645128971170deeff9d9af5b36d2c15a338fd71
Ge	PAW_PBE Ge_d 03Jul2007	944b26c40d2d7c4f4eb1ff3a2e8dbfdd7129146276cd341854bfd5c0e57780ed

El.	TITEL	SHA
H	PAW_PBE H 15Jun2001	030f79b5d3ab3cf0e668861823c8fb652ff669f3e15e46930bd03bfd63a607b6
He	PAW_PBE He 05Jan2001	767818bb8a862153b2ebc238b4abd4bed99a882bbb8e6a4800cddfa4f1a760c3
Hf	PAW_PBE Hf_pv 06Sep2000	326372999ee61732e8151b0274b0330bf639aff42dca34b327393d3d5ff5d3de
Hg	PAW_PBE Hg 06Sep2000	b58054e5facb8a6c456f8fea289fc655b681c0fa06131ba074282c377c596e89
Ho	PAW_PBE Ho_h 29Jun2022	f964032ac636ca1bab774bb902286f5c66af571df067f67ca2e3f0edddb1c51
I	PAW_PBE I 08Apr2002	e40f3f59b681c1fc3e3091736183c4589116986673d2b852a5012aec72758799
In	PAW_PBE In_d 06Sep2000	bef4eefb233e1f458c7ef2e09e39e7114bb5a6a38c7ac356915527764429c513
Ir	PAW_PBE Ir 06Sep2000	7c6af8d4d487b237782eb51e6f62977b27a1da78c3c96acd1cebefd6c308f120
K	PAW_PBE K_sv 06Sep2000	bf8373ef592e31d27efa2dcc68371be6d6a25ce4db6c2ffaf9e92c44050ba21a
Kr	PAW_PBE Kr 07Sep2000	6b89d4ab453c74a018c642cd8d7c9a2bec7c33c7e53fbff7492fc5bbd2c9051e
La	PAW_PBE La 06Sep2000	b7aad99517e50aeb53363b20a29bb0dfa896544080812fb23322f071df953199
Li	PAW_PBE Li_sv 10Sep2004	7e51fe1804c037e1dccc81a9c376d94d693a7559600c847f4b41960edb8ab895
Lu	PAW_PBE Lu_3 06Sep2000	fe1f8b446106b829a34406137eadf9babd792fb03d1986447d054dbaf8059d6c
Mg	PAW_PBE Mg_pv 13Apr2007	f474ac0dd33840b9ae76c01d57fea79fdf77cdfbb07d5ade72c65f83c709b62b
Mn	PAW_PBE Mn_pv 02Aug2007	c79df11ab18a0e3347296df6ded47bb5f18b2e4fbd621d0b5280d2eae24c30a0
Mo	PAW_PBE Mo_pv 04Feb2005	6ae1433eb25a8c9ce9b558610a2d5a3c8775e861c8272ad13d852ff7f9633ae0
N	PAW_PBE N 08Apr2002	e053789ff3a61a86a1b75d8a110fcc91f86041011e7b0817c7c99e4e8a6349d7

El.	TITEL	SHA
Na	PAW_PBE Na_pv 19Sep2006	6a2f546d9e11350984debacf3dc457d8cffc0868e817d445faca461816a32b94
Nb	PAW_PBE Nb_pv 08Apr2002	bac2b60850b34f8515cf56f9feae68b678e347865051052a0e1f5d2c6a691c0a
Nd	PAW_PBE Nd_h 01Jun2022	7bd4bb7cee51b5dc2e0f9cbae2e86e657034401e01318a3a9244a0deed38a434
Ne	PAW_PBE Ne 05Jan2001	7551ec1d38f079f813f98269ad695dc650bd9c34a5dedf814d6a76328defc8c0
Ni	PAW_PBE Ni_pv 06Sep2000	368cd815a19284a5fda64519f43fef792dad8376deb9e2da41aae78b997dc50e
Np	PAW_PBE Np 06Sep2000	ccc3f89c89c668b33a1cedb3a141ff87191bee6923db3e8755910d8c985d3af2
O	PAW_PBE O 08Apr2002	818f92134a0a090dccd8ba1447fa70422a3b330e708bb4f08108d8ae51209ddf
Os	PAW_PBE Os_pv 20Jan2003	df2e3ef880fc2502babe687ce20ec2e4b82fab5eb8dd3b5c0a23d3b7861e7a8b
P	PAW_PBE P 06Sep2000	df60c54a93efe35c9e85ae94c010c75e9f6960a95d5595d7cdba4096d109af88
Pa	PAW_PBE Pa 07Sep2000	04e32654b760de29c7f02015f2c4b9b92aeb120699210996a29249ba80bfa323
Pb	PAW_PBE Pb_d 06Sep2000	fb885b08f0fba73a15f6a6b0e39bd200c13ec96ef97cf3ecd8e63bade5137abd
Pd	PAW_PBE Pd 04Jan2005	dd6f6f02930356371984e2b707ff5e456046761dc76b07c1eba30abd15eb3c39
Pm	PAW_PBE Pm_h 01Jun2022	e20fde408f4bc5ec1ab6d6cec4ca07cb81fc0f789787f0fe8d07d98759b2aec6
Po	PAW_PBE Po_d 25May2007	589bb7cf7db41d81724fa452df1c3d870736441cf2fe2863a84270f4db2d0320
Pr	PAW_PBE Pr_h 01Jun2022	0607a17d0060e989022cd48f8f145dff5f704ed14e44fe020789997c290d1ea3
Pt	PAW_PBE Pt 04Feb2005	3ed90460adef76debccff1cfb73ee1349b515b1a3db03439735b44de3a8db7dc8
Pu	PAW_PBE Pu 06Sep2000	aea5004a3542f2b7cbf52448d5c3d9b9e438d6248055eeb36c781f43d2b3cf3c

El.	TITEL	SHA
Ra	PAW_PBE Ra_sv 29May2007	c89b71e1d92b290ba352aa2322e5ac7f7cc2f71bf48f725710403fd01d027668
Rb	PAW_PBE Rb_sv 06Sep2000	06c38fe1ec7709d96d3959f5f2c66fec330a93b52b042a8fb2dfe6a3a3fb06c1
Re	PAW_PBE Re_pv 06Sep2000	9136fabd3a1e35b9fb4b1f356ef358c338d3d4e46f3e96ab15e45974af27d0c0
Rh	PAW_PBE Rh_pv 25Jan2005	25b11608b0d10a93adcc8487bc062d7eb8aeda443ca523c31dcc1b5e75119ef1
Rn	PAW_PBE Rn 12Aug2016	1082a7f1e478858715023a6a817d2c8d5512517dec9bddb12f27eca6306ec2cc
Ru	PAW_PBE Ru_pv 28Jan2005	539bee49bb4e63d8933d8244c4f66bec34c4e5cbe2759ec5d366ad1017752494
S	PAW_PBE S 06Sep2000	0fc7481fb0695f01bdc6462160264c5c84044ae9ec85a907d398b887a2bc3132
Sb	PAW_PBE Sb 06Sep2000	8a1325a3afd8ca988779475cff04188eb880a428d1acb53275fe456fa3b784fc
Sc	PAW_PBE Sc_sv 07Sep2000	9aad5a0618293b7e22b0823afd8bf80ef5c5e525eb8618ba91672918e18a06fa
Se	PAW_PBE Se 06Sep2000	eabb916e6b4c819dc065ce039373bc328651da483898f08fb9e49c498452bf12
Si	PAW_PBE Si 05Jan2001	79d9987ad8750f624c4d6acb2a16d13abf6a777132adc04dc6c8399be72b42bb
Sm	PAW_PBE Sm_h 30May2022	2f62dec1b7198d20317f663b75f15c0d34872d9e465e7140f969bed2fb3252a3
Sn	PAW_PBE Sn_d 06Sep2000	385b269c1887fa92a2bd1b595c4ea1490c7eb92f9f3d87257729a4a813cde741
Sr	PAW_PBE Sr_sv 07Sep2000	a8389d3481648516ee67182ee030b298d280b37e29cbbf2d8595f040d757c710
Ta	PAW_PBE Ta_pv 07Sep2000	00d0a14a36c127416459414afb8617d9754996ffa60a2465888e660b20a452f
Tb	PAW_PBE Tb_h 30May2022	1b65b31de2c27578bdfaaa2be6c07419aa8a7e4c6a2be444d54e32093864b0c5
Tc	PAW_PBE Tc_pv 04Feb2005	55d1e894bb6e22d412434369d62e29007ee0956d7c4b4ca346dcdb73d72337c9

El.	TITEL	SHA
Te	PAW_PBE Te 08Apr2002	e13b0861f25acb1fe6cdc17458a3647985498b67a429eb77ddc1eac05a1775b1
Th	PAW_PBE Th 07Sep2000	d41e9f824f712d7814b19b6bc43381cc9a373f2ab99e53c63e55d3471ac6bd23
Ti	PAW_PBE Ti_pv 07Sep2000	f757a1b2c6d082f4c628fa3d987464a8763bf92e53844ac0500b0e2ddc9ce5c0
Tl	PAW_PBE Tl_d 06Sep2000	114f54bd8cac727af4c1a2dcc375cc6f82ae0f808e1efd36f54552a740d0afeb
Tm	PAW_PBE Tm_h 29Jun2022	14c2249a7b2afb252acd0daad4b9c552cb4fdb549ec5080ecaac209e82a28e2c
U	PAW_PBE U 06Sep2000	83ff4a3ef579a1d3def1e25ae1b036f9320912559a2f473c33031cce813da2e2
V	PAW_PBE V_pv 07Sep2000	1175d3c8cb4ffd1d150a520fa74fae5c3ec72c0849b5615a94a5372dd2cf07f7
W	PAW_PBE W_sv 04Sep2015	931c2d770f65867ef30f3db3421922900fc0890ebac5c3e12f63b6a2064023d7
Xe	PAW_PBE Xe_GW 08Jan2009	d550ac1633c6a0fdbf4cc3b9e9481b749e6bbfc02e3e0a4eed1c4f3493688506
Y	PAW_PBE Y_sv 25May2007	5e7f7496c6fa99024fec326bcd60dcee8ff7e886f9613d31da35c685a538a036
Yb	PAW_PBE Yb_h 29Jun2022	cfae7690412fd84d754fbf73d8a1e0d0ef26063421fabf4cb7e6c45490da7400
Zn	PAW_PBE Zn 06Sep2000	501fddb8274dd8e9725d4f3de27861d7f1e553a7e18441bc79fed8f346e7f23
Zr	PAW_PBE Zr_sv 04Jan2005	25aed69cb10325f9d37c5c68912b61a17387d1f8e4f1d804860ffa10c8a4bf76

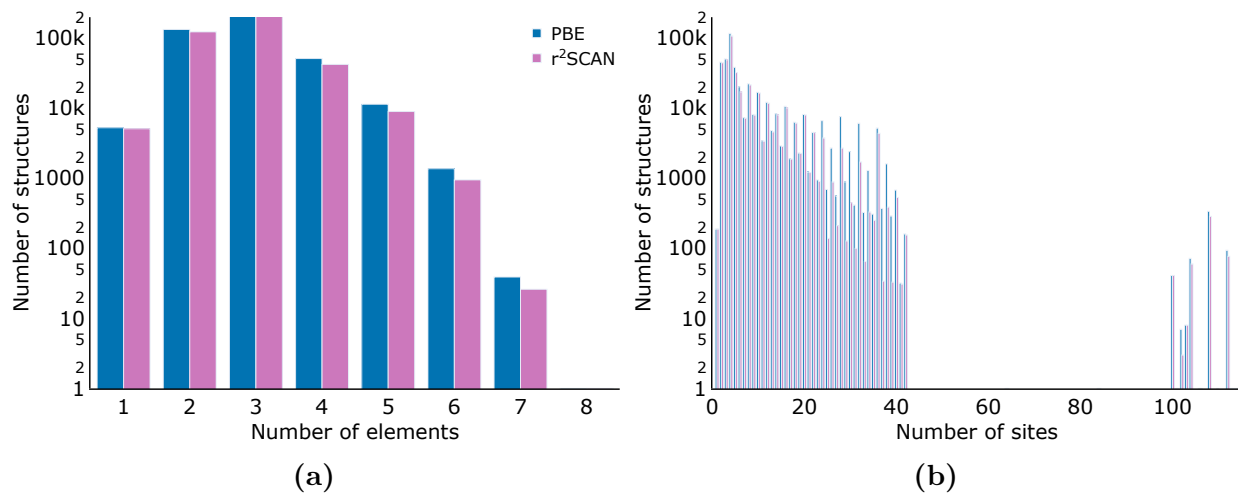


Fig. S10: Distribution of the number of elements (a) and number of sites (b) for the MatPES structures. The number of structures for a given quantity are plotted on a logarithmic scale. The blue (purple) bars show the structure counts for the PBE (r^2 SCAN) subsets of MatPES.